



# Scale dependency in quantifications of the avulsion frequency of coastal rivers

Luca Colombera<sup>\*</sup>, Nigel P. Mountney

Fluvial, Eolian & Shallow-Marine Research Group, School of Earth & Environment, University of Leeds, LS2 9JT Leeds, UK

## ARTICLE INFO

### Keywords:

Fluvial  
Delta  
Holocene  
Backwater  
Autogenic  
Lobe switching

## ABSTRACT

Quantification of the frequency with which coastal-plain rivers avulse is important for elucidating autogenic dynamics and their role as controls on landscape change and stratigraphic architectures. An outstanding question exists, however, as to whether measures of avulsion frequency are inherently affected by the spatial and temporal scales at which they are evaluated, which has implications regarding our ability to make direct comparisons between different river systems or deltas. To address this problem, a quantitative analysis of the avulsion histories of 57 coastal-plain river systems is undertaken. Nine alternative measures of avulsion frequency are extracted. These are based on numbers of (i) avulsion events, (ii) active or abandoned channel courses, and (iii) delta lobes, all considered per unit time. Additional sets of avulsion-frequency proxies are established based on normalization of these numbers relative to the size of the area being studied, and to the number of distinct river systems that drain into that area. The sensitivity of these quantities to the spatial and temporal extent of study areas and time intervals, and their relationships with quantities describing the scale of the river systems, are assessed. All avulsion-frequency estimates demonstrate apparent negative relationships with the timespan over which they are determined; this may reflect global Holocene trends, or variations in resolution with the time window. Avulsion metrics that are not normalized by the planform extent of the study area do not show proportionality with the size of the study areas themselves, nor with the scale of the river systems; correspondingly, the spatio-temporal density of avulsion events tends to be higher for smaller rivers and associated study areas. This may be due to systematic variations in data resolution, to the influence of external controls that relate to the scale of deltas, or to inherent non-stationarity in the avulsion dynamics of lowland rivers, in association with forms of self-organization that do not vary with scale. Although non-normalized avulsion-frequency estimates do not scale with measures of river-system size, they are seen to correlate with progradation rates, which are themselves scaled to sediment discharge and catchment size. Practical considerations can be drawn on how avulsion frequency may be appropriately quantified to enable meaningful comparisons of the autogenic dynamics of coastal-plain rivers.

## 1. Introduction

Channel avulsion resulting in the diversion of a channelized sediment-transport pathway in favour of a new course is a common process of rivers, alluvial torrents and submarine channels (e.g., McCarthy et al., 1992; Field, 2001; Colombera and Bersezio, 2011; Jobe et al., 2020). Quantifications of the frequency with which channels avulse are crucial for research aiming to improve our understanding of (i) landscape change associated with channel morphodynamics, (ii) the role of autogenic mechanisms in governing the spatio-temporal variability in sediment distribution in sedimentary basins, and (iii) controls on the architecture of sedimentary successions (e.g., Bryant et al., 1995; Pelletier and Turcotte, 1997; Jerolmack and Mohrig, 2007; Gouw,

2008). However, the quantification of the frequency of avulsion events is not trivial. This quantification is commonly expressed in terms of interavulsion period, i.e., the lifespan of a channel, or its reciprocal value, the avulsion frequency (Törnqvist, 1994; Stouthamer and Berendsen, 2001; Törnqvist and Bridge, 2002; Slingerland and Smith, 2004). Yet, it can be surmised that these quantities depend on the spatial scale of the sample on which they are based (e.g., a reach of a certain length, a delta plain, an entire river system). In particular, these quantities depend on the total, cumulative channel length considered, which is itself a function of the extent of the area being evaluated and of the density of the channel network contained therein (cf. Stouthamer and Berendsen, 2007). This supposed dependency of avulsion frequencies on spatial scale has implications for the ability to make direct comparisons

<sup>\*</sup> Corresponding author.

E-mail address: [l.colombera@leeds.ac.uk](mailto:l.colombera@leeds.ac.uk) (L. Colombera).

<https://doi.org/10.1016/j.earscirev.2022.104043>

Received 1 November 2021; Received in revised form 20 April 2022; Accepted 2 May 2022

Available online 6 May 2022

0012-8252/© 2022 The Authors. Published by Elsevier B.V. This is an open access article under the CC BY license (<http://creativecommons.org/licenses/by/4.0/>).

between different channelized systems. Equally, quantifications of the frequency of avulsion events may also vary depending on the temporal window over which they are determined. For datasets detailing Holocene avulsion histories, this may happen in part because of variations in avulsion frequency through time, in relation to temporal variations in the influence of geological controls, and in part because of the increased difficulty in resolving avulsion records as we consider progressively older episodes of river-system evolution. In considering the potential relationships between avulsion-frequency quantifications and the scales over which they are made, a question arises as to whether these quantities may be affected by factors whose importance is known to scale to the size of the sediment-routing system. For coastal-plain rivers, in particular, the scale of the fluvial system dictates characteristics such as the dominant sediment-delivery mechanisms, the streambed gradient, the extent of the backwater zone, and the rate at which the shoreline progrades (Milliman and Farnsworth, 2011; Blum et al., 2013; Aadland and Helland-Hansen, 2019). These factors can all influence the avulsion frequency of coastal channels, for instance by exerting controls on streambed aggradation and development of cross-channel gradient advantages (Jones and Schumm, 1999; Slingerland and Smith, 2004). On this basis, it can be hypothesized, for example, that larger river systems, typically associated with faster river-mouth progradation and gentler streambed gradient, may be prone to experience more frequent channel avulsions. At the same time, however, larger deltas may be characterized by less erodible delta-plain substrates, which may on the contrary offer increased resistance to channel diversions (cf. Edmonds and Slingerland, 2010). It is therefore of interest to establish whether some inherent scaling exists between avulsion frequencies and river-system scale. Given the particular set of scale-dependent variables that may control avulsion dynamics in lowland rivers, the focus of this work is specifically on fluvial systems that developed in relative proximity to the coast.

The aim of this work is to establish the degree to which avulsion-frequency metrics may depend on the temporal and spatial scales of investigation. Specific research questions are as follows. What quantification is needed to enable meaningful comparisons of avulsion frequencies relating to different river systems? If these metrics are seen to vary across spatio-temporal scales, what are the possible methodological and geological explanation of apparent variations? Given the inherent covariance of factors that are linked to river-system scale, and considering how these variables act to control river avulsion, is avulsion frequency intrinsically dependent on river-system size?

What this work does not aim to achieve is a comprehensive assessment of controls on avulsion frequencies, which are partly determined by factors that act independently of scale. Nevertheless, to understand whether potential dependency of avulsion frequency on scale is an apparent (i.e., due to methodological reasons) or true (i.e., due to geological reasons) phenomenon, we need to consider the role of potential geological controls that could cause it.

## 2. Data and methods

### 2.1. Original literature data

The dataset that underpins the quantifications presented in this work consists of qualitative documentations of the Holocene avulsion histories of 57 case studies of river deltas and alluvial coastal plains (Table 1; Fig. 1A). These examples were chosen based on the availability of suitable data documenting avulsion histories, channel activity and/or delta-lobe development over known temporal intervals. The case studies include both marginal-marine and marginal-lacustrine examples. Collectively, they cover a broad range of river-system scales (five orders of magnitude in drainage-basin area; Fig. 1B). The selected marginal-marine examples also developed under varied process regimes, i.e., they differ with respect to the relative importance of fluvial, wave and tidal processes in shaping their morphology and controlling their evolution (Fig. 1C); however, the dataset is characterized by a

predominance of river-dominated settings (28, compared to 17 wave-dominated ones and 3 tide-dominated ones), which may not be representative of deltaic systems globally (cf. Nienhuis et al., 2020). All the data are derived from open-source scientific literature (articles, dissertations, reports). The original studies documented the temporal evolution of lowland rivers through variable time spans of the Holocene. The planform evolutions of these river systems were characterized in terms of one or more of the following aspects: (i) courses of abandoned channels (palaeochannels), as well as presently active ones, (ii) location of avulsion sites and events, and/or (iii) position and extent of delta lobes. The occurrence of these features was variably determined on the basis of evidence available through historical maps or records (e.g., Bondesan et al., 1995; Mateo and Siringan, 2007), remote sensing (including satellite images, aerial photos, LiDAR or InSAR elevation data; e.g., Serrano Suarez, 2004; Phillips, 2012; Syvitski et al., 2013; Haghani and Leroy, 2020), and field investigations providing data on surface geomorphology and on the shallow subsurface geology (based on borehole and geophysical observations; e.g., Berendsen and Stoutamer, 2002; Fielding et al., 2006; El Bastawesy et al., 2017). The Holocene histories were reconstructed based on available temporal constraints: radiometric dates (e.g., Muñoz-Salinas et al., 2017), historical accounts (e.g., Holmes, 1968), archaeological evidence (e.g., Stanley et al., 2004), and historical maps, satellite images or aerial photos of known age (e.g., Karymbalis et al., 2016). Where multiple suitable data sources existed for the same case study, the datasets were integrated into a single reconstruction, if possible. Where discrepancies existed in the interpretations of Holocene histories based on different datasets available for the same case study, the interpretations that were considered were those supported by the most robust evidence and associated with higher-resolution data in terms of recognition of geological features and/or chronological constraints. Chronometric data were sourced from the wider literature, additional to the data sources on planform changes. All primary data sources are reported in Table 1.

### 2.2. Approaches to the quantification of avulsion frequency

Some alternative ways to quantify the frequency of river avulsion were considered, based on three fundamental quantities: (i) the number of avulsion events that occurred during a time interval, (ii) the number of channels that were active during a time interval, and which may or may not have been abandoned during that time (active channels and palaeochannels are collectively referred to as ‘channel threads’ hereafter), and (iii) the number of delta lobes that were active, and which may or may not have been abandoned, during a time interval (Fig. 2). For each case study, the time intervals considered for each quantification may differ, depending on the available records of each type of quantity. These numbers were determined over a study area of given size, typically the entire delta plain or the portion of a coastal plain that was active during the specified time (referred to as ‘study area’, hereafter). The size of the study areas is in part dictated by data coverage; hence, for each case study, the considered area may have differed for the three forms of quantification. In some cases, the defined study areas cover regions that are now located at considerable distance from the present-day coast: this is because study areas are defined to capture river reaches that developed in proximity of the shoreline in the past, and many of the studied examples have undergone extensive shoreline progradation over the timescales of interest.

The number of avulsion events considered includes both ‘full’ and ‘partial’ avulsions of reaches that lead to a river mouth; full avulsions consist of channel diversions that lead to the abandonment of a reach, whereas partial avulsions represent events that cause the establishment of a new course that coexists with the antecedent one (Slingerland and Smith, 2004). Events of levee break forming crevasse splays or subdeltas that are only active at high flow stage are not considered as avulsion events. Neck and chute cutoffs, which occur within the boundaries of channel belts, are not treated as avulsions. The avulsion events

**Table 1**

Summary of the case-study coastal-plain river systems considered in this work, of the types of avulsion metrics extracted for each, and of the primary data sources. Ticks that appear in brackets indicate avulsion, channel-thread or delta-lobe records that are thought to be incomplete, and therefore examples that likely yield underestimated quantities.

ID	River system	N avulsion events	N channel threads	N delta lobes	Data sources
1	Saskatchewan upper delta	✓	✓		Morozova and Smith (1999, 2000)
2	San Antonio-Guadalupe	✓	✓	✓	Donaldson et al. (1970); McGowen et al. (1976); Weinstein and Junkin (1992); Phillips (2012)
3	Grijalva	✓	✓		von Nagy (2011); Nooren (2017)
4	Usumacinta	✓	✓		von Nagy (2011); Nooren (2017); Muñoz-Salinas et al. (2017)
5	Mississippi	(✓)	✓	✓	Welder (1955); Törnqvist et al. (1996); Roberts (1997); Chamberlain et al. (2018); Bhattacharya et al. (2019)
6	Sinú	✓	(✓)		Serrano Suarez (2004)
7	Orinoco	(✓)	(✓)		Van Andel (1967); Aslan et al. (2003)
8	Goose	✓		✓	Nijhuis (2013); Nijhuis et al. (2015)
9	Parafba do Sul		✓	(✓)	Martin et al. (1993); Da Rocha (2013); Ainsworth et al. (2019)
10	Doce		✓		Martin et al. (1993); Rossetti et al. (2015)
11	Jequitinhonha		✓	✓	Martin et al. (1993); Dominguez et al. (1981); Martin et al., 1993; Ainsworth et al. (2019)
12	Turia		✓		Ruiz-Pérez and Carmona (2019)
13	Ebro	✓	✓	✓	Somoza et al. (1998); Somoza and Rodríguez-Santalla (2014)
14	Llobregat		✓		Gàmez Torrent (2007)
15	Rhône	(✓)	✓	✓	Rey et al. (2009); Fanget et al. (2014); Provansal et al. (2015)
16	Rhine-Meuse	✓	✓		Berendsen and Stouthamer (2002); Stouthamer et al. (2011)
17	Po	✓	✓	✓	Bondesan et al. (1995); Mackey and Bridge (1995); Correggiari et al. (2005a, 2005b)
18	Catumbela		✓		Dinis et al. (2018)
19	Acheloos		✓		Piper and Panagos (1981); Vött et al. (2007a, 2007b)
20	Evinos		✓		Piper and Panagos (1981); Maroukian and Karymbalis (2004)
21	Mornos		✓		Karymbalis et al. (2007); Parcharidis et al. (2013)
22	Selinous		✓		Kontopoulos and Avramidis (2003); Koutsios et al. (2010)
23	Aliakmon		✓		Ghilardi (2007); Ghilardi et al. (2008); Styllas (2018)
24	Pinios		✓		Gaki-Papanastassiou et al. (2010); Karymbalis et al. (2016)
25	Axios		✓		Ghilardi (2007); Ghilardi et al. (2008)
26	Lilas	✓	✓	✓	Karymbalis et al. (2018)
27	Asopos	(✓)	✓	(✓)	Gaki-Papanastassiou et al. (2011); Gaki-Papanastassiou (pers. comm.)
28	Danube	(✓)	(✓)	✓	Vespremeanu-Stroe et al. (2017a, 2017b)
29	Nile		✓		Stanley and Warne (1993); Stanley et al. (2004); El Bastawesy et al. (2020)
30	Mfolozi	✓	✓		Grenfell et al. (2009)
31	Ceyhan-Seyhan	(✓)	✓	(✓)	Erol (2003); Ataol (2015); Rutishauser et al. (2017)
32	Sulak		✓	(✓)	Mikhailov et al. (2004, 2012)
33	Karkheh	(✓)	✓		Heyvaert et al. (2012)
34	Shatt-al-Arab		✓		Hussein (2011); Heyvaert and Walstra (2016); Al-Hamad et al. (2017)
35	Sefidrud	(✓)	✓	(✓)	Kazancı et al. (2004); Kazancı and Gulbabazadeh (2013); Haghani and Leroy (2020)
36	Indus		✓		Holmes (1968); Syvitski et al. (2013)
37	Ili		✓		Abdrasilov and Tulebaeva (1994); Deom et al. (2019)
38	Cauvery		✓		Ramasamy et al. (1991); Ramasamy et al. (2006); Singh et al. (2015)
39	Palar		✓		Ramasamy et al. (2006); Resmi et al. (2017)
40	Krishna		✓	✓	Nageswara Rao et al. (2020)
41	Godavari	✓	✓	✓	Nageswara Rao et al. (2015)
42	Mahanadi		✓		Mahalik et al. (1996); Maejima and Mahalik (2002); Dash et al. (2020)
43	Bengal (Ganges-Brahmaputra)		✓	(✓)	Allison et al. (2003); Sarker et al. (2013); Akter et al. (2016)
44	Irrawaddy	(✓)	✓	(✓)	Kravtsova et al. (2009); Giosan et al. (2018); Chen et al. (2020)
45	Red River (Song Hong)		(✓)	✓	Mathers and Zalasiewicz (1999); Tanabe et al. (2006); Cuong (2009); Funabiki et al. (2012)
46	Selenga	✓			Dong (2020)
47	Yellow River (Huanghe)	✓	✓	✓	van Gelder et al. (1994); Ganti et al. (2014); Wang et al. (2016); Zheng et al. (2017); Moodie et al. (2019)
48	Luanhe	(✓)	✓	(✓)	Wang et al. (1986); Cheng et al. (2020); He et al. (2020)
49	Tseng-wen	✓	✓		Chang and Chen (2001)
50	Pa-chang	✓	✓		Chang and Chen (2001)
51	Agno-Dagupan	(✓)	✓	✓	Mateo and Siringan (2007)
52	Bued-Patalan		✓	✓	Mateo and Siringan (2007)
53	Mary		✓		Mulrennan and Woodroffe (1998)
54	McArthur		✓		Woodroffe and Chappell (1993); Jones et al. (2003)
55	Gilbert		✓		Nanson et al. (1991); Jones et al. (2003)
56	Mitchell	✓	✓	(✓)	Lane et al. (2017)
57	Burdekin		✓	✓	Fielding et al. (2005a, 2005b, 2006)

considered in the quantification correspond to those that are significant enough to be recorded in the data sources (Table 1); as such, resulting metrics suffer from some subjectivity and are likely to represent conservative estimates. The number of avulsion events could be obtained for 28 of the 57 case studies; however, avulsion counts are thought to be accurate estimations of a true total number for 17 examples only.

The number of channel threads includes all the river courses leading to a river mouth that were active during the considered timespan, including those that may have been activated before. All throughgoing channel courses that are mapped and inferred to have been hydrologically connected to the river are included, regardless of their size. Inclusion of channels that may have already been active was done to

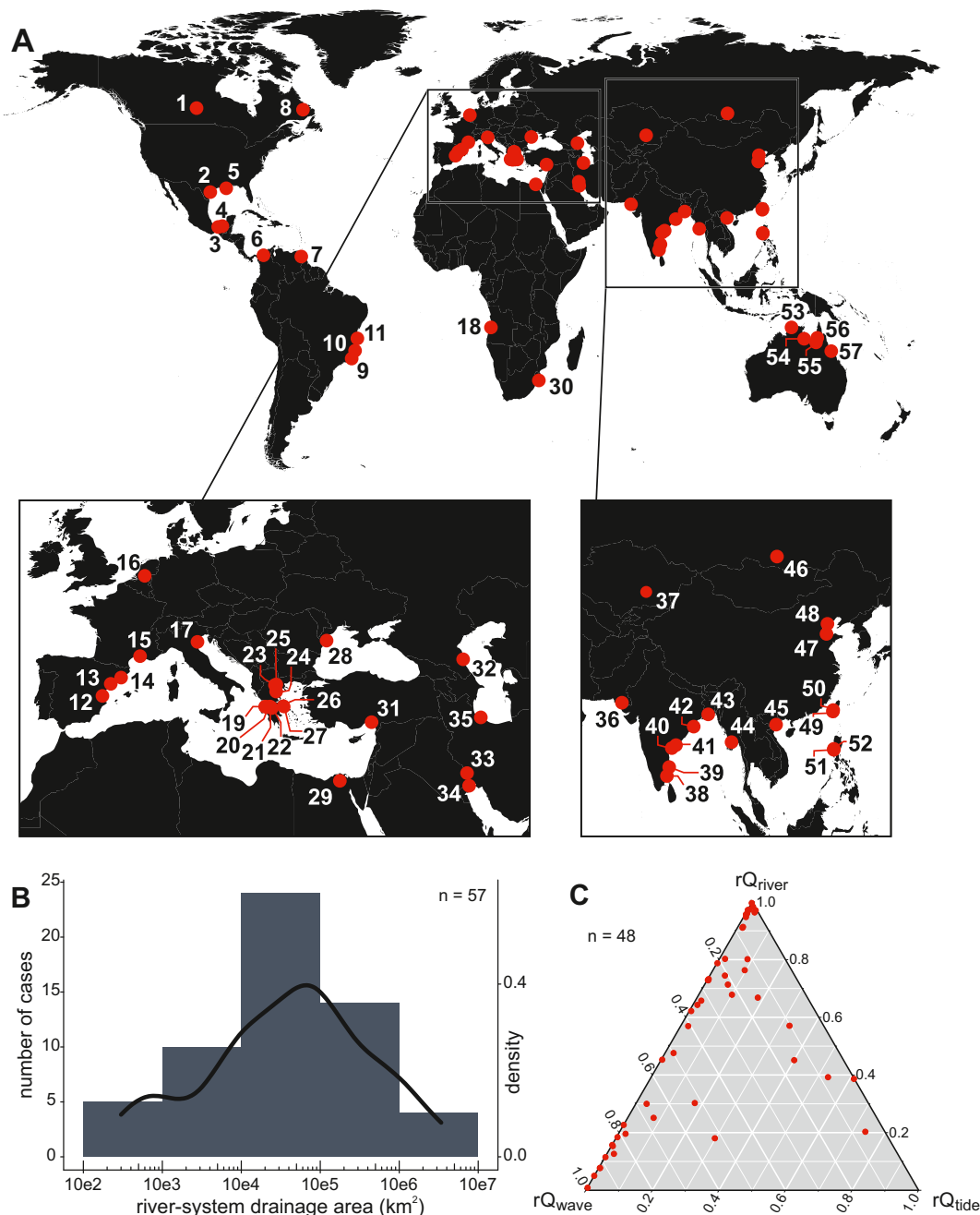


**Fig. 1.** (A) location map of the coastal-plain river systems considered in this study. (B) histogram and kernel density estimation of the distribution of drainage areas of river systems considered in this study; note the logarithmic scale in abscissa. (C) Ternary diagram illustrating the variability in process regime of marine deltas included in the study, expressed in terms of relative sediment flux ( $rQ$ ) associated with river, wave and tidal processes, based on data from [Nienhuis et al. \(2020\)](#). All presented data are included in the Supplementary Material.

broaden the temporal window of the observations as much as possible, as the exact timing of activation of older palaeochannels is in many cases unknown. However, this poses an issue in that the number of channel forms whose activation pre-dated the studied temporal interval may vary across the studied river systems. This quantity also includes channel threads that may have been established through avulsions that took place outside of the study area. Palaeochannels that are known to have been born from bifurcations around mouth bars at the coast, and which may have been incorporated into the delta plain following shoreline advance, have been excluded. As defined in this work, the term ‘channel thread’ is used to refer to individual distributary courses, which may take the form of channel belts with multiple channels: a braided channel belt is counted as one single ‘channel thread’. The number of

channel threads could be obtained for 54 of the 57 case studies, 51 of which are considered to have been characterized comprehensively.

The number of delta lobes quantifies the number of avulsions that are significant enough – in terms of magnitude of river-mouth relocation – to cause lobe switching. For the scopes of this work, a ‘delta lobe’ is defined as a three-dimensional sediment volume made of cogenetic delta-top, delta-front and prodelta deposits associated with a particular state of the drainage network that arose because of river avulsion (cf. [Colombera and Mountney, 2020](#), and references therein). Different diagnostic criteria may have been considered in the original data sources for the definition of delta lobes, such as the recognition of prodelta to delta-top facies successions, the lenticular three-dimensional shape of sediment accumulations, or some preserved seaward protrusion in

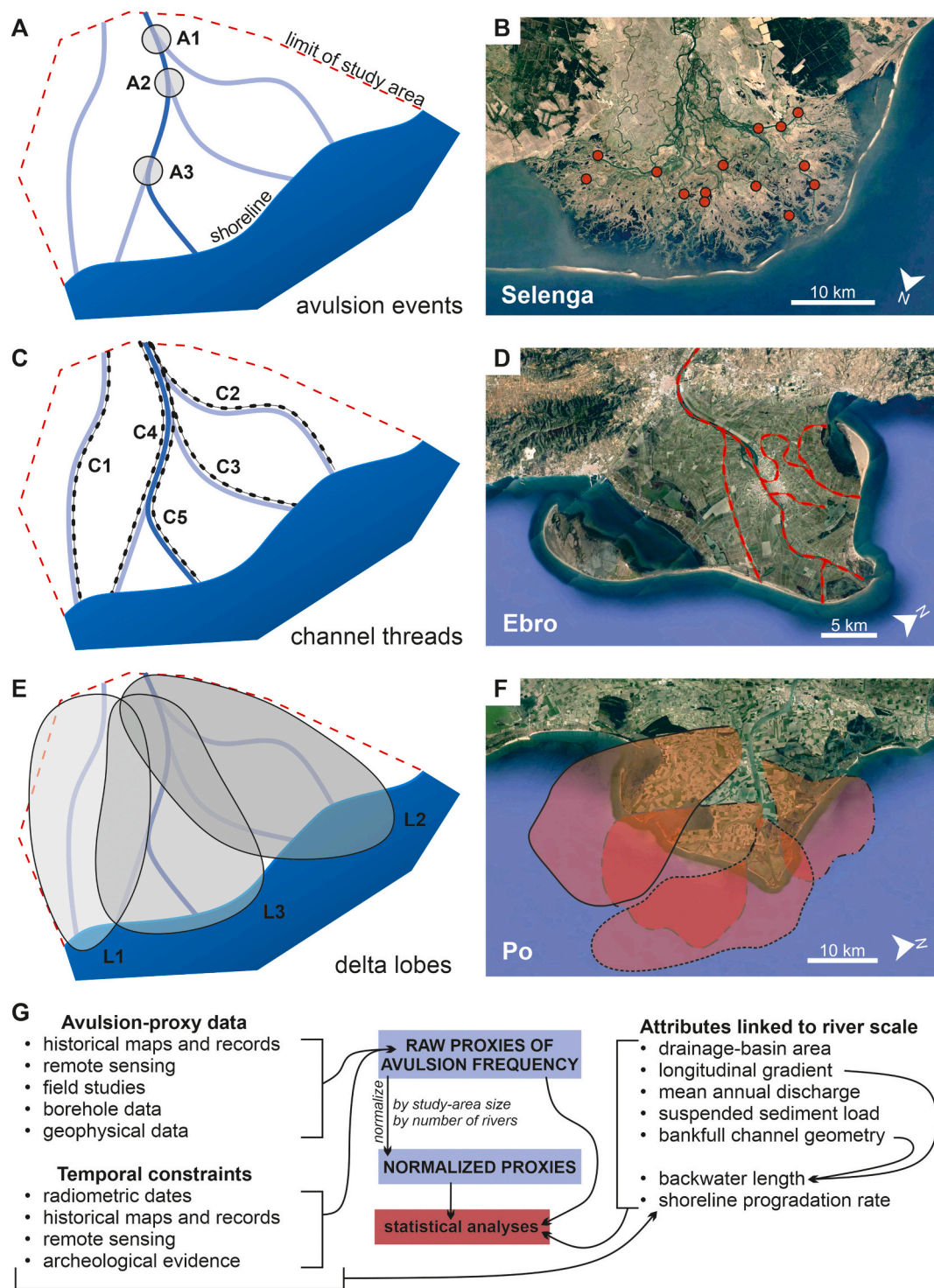


**Fig. 2.** Depiction of the features used to define the avulsion-frequency metrics used in this work: (A) idealized example of counted avulsion events and (B) their recognition in one of the case studies, the Selenga River delta (cf. Dong, 2020); (C) idealized example of counted channel threads and (D) their recognition in the Ebro River delta (cf. Somoza and Rodríguez-Santalla, 2014); (E) idealized example of counted delta lobes and (F) their recognition in the Po River delta (cf. Correggiari et al., 2005a); (G) flow-chart summarizing the adopted workflow and data types.

planform, related to abandoned river mouths. The chosen definition of a delta lobe can be applied at different scales to units that may even be nested hierarchically. The data were extracted relying on the application of the term ‘delta lobe’ by the authors of the original datasets; doing so means considering entities that are not necessarily comparable in terms of scale of development, but permits this category to be applied objectively. Accounts of delta lobes exist for 25 of the 57 case studies, but

numbers of delta lobes developed over a known length of time are only thought to be comprehensive for 16 of these.

The numbers of avulsion events, channel threads, and delta lobes per unit time are each considered as alternative proxies for channel avulsion frequencies. In addition, all these quantities are normalized relative to the planform extent of the study area considered for each. This permits determination of avulsion ‘density’, describing the number of avulsion

events, channel threads or delta lobes both per unit time and per unit area. The study area considered for this type of normalization corresponds to the coastal-plain area of interest covered by the river system up to the present day: i.e., currently drowned delta lobes are included, whereas any change in area due to coastal progradation is not quantified. These metrics are referred to as rates normalized by area, hereafter.

Some additional normalization has also been applied to the avulsion metrics of eight examples, representing the Holocene histories of coastal plains traversed by multiple coalescing river systems that joined intermittently. The quantities are normalized by the maximum number of river systems with distinct catchments known to have had independent drainage to the sea or lake at some point during the considered evolutionary histories; this value ranges from one, for the 49 examples not requiring normalization, to four. These metrics are referred to as rates normalized by area and river number, hereafter.

### 2.3. Ancillary data and associated quantifications

Ancillary data have been collected to constrain variables that describe the river systems and that are known to scale with their size. Among these, the variables considered in this study are: (i) river-system drainage-basin areas, (ii) average river water-surface gradients across the study areas; (iii) mean annual water discharges as based on observations from gauging stations located near the upstream end of the study area (data from the *Global Runoff Data Centre*, from the primary data sources of Table 1, and from the wider scientific literature: Begg, 1978; Poulos and Chronis, 1997; Fytianos et al., 2002; Kao and Milliman, 2008; Milliman and Farnsworth, 2011; Cohen et al., 2013; Efstratiadis et al., 2014; Pueppke et al., 2018; Skoulikidis et al., 2018; Nienhuis et al., 2020), (iv) suspended sediment loads (data from the primary data sources of Table 1 and from the literature: Ashmore and Day, 1988; Poulos and Chronis, 1997; Rivera, 1997; Erkens et al., 2006; Syvitski and Saito, 2007; Kettner and Syvitski, 2008; Rustomji, 2010; Bernardes et al., 2012; Milliman and Farnsworth, 2011; Potemkina, 2011; Cohen et al., 2013; Duskayev et al., 2020), (v) empirical estimations of bankfull width and mean bankfull depth at the upstream end of the study area, as provided by Andreadis et al. (2013). Where available, data on water discharge and sediment load have been used that relate to times prior to the construction of dams, which may have significantly altered these quantities.

Shoreline progradation rates are calculated as increases in coastal-plain area per unit shoreline width per unit time; these rates are computed based on temporal constraints available in the scientific literature, and over a timescale of equivalent order of magnitude to that of one or more of the avulsion-frequency proxies computed for each case study.

Backwater lengths are estimated as the ratio between flow depth at the upstream end of the study area and the water-surface gradient across the study area, which is considered to be a reasonable approximation of the streambed gradient (cf. Paola, 2000). Alternative quantifications of backwater lengths are computed according to three different approaches based on (i) mean bankfull depth (Andreadis et al., 2013), (ii) a characteristic flow depth based on mean yearly discharge and bankfull width (cf. Lamb et al., 2012), and (iii) a characteristic flow depth determined from the mean discharge of the wettest month and bankfull width (cf. Chatanantavet et al., 2012; Lamb et al., 2012; Ganti et al., 2016a). Results of the application of the three approaches have been compared with each other, as well as with other estimations of backwater lengths for the same coastal rivers (Jerolmack, 2009; Chatanantavet et al., 2012; Ganti et al., 2016b; Hartley et al., 2017). This was done to establish the sensibility of the quantifications. As the three chosen approaches yield similar results, for scopes of data presentation, only backwater-length estimations based on inferred mean bankfull depths are presented, since these could be constrained for the largest number of case studies (N = 50).

### 2.4. Dataset limitations

Each of the chosen alternative approaches to the quantification of avulsion frequency suffers from some issues. All the metrics may be affected by some degree of human regulation of the river systems, especially in the form of controls on river drainage and efforts for preventing river avulsions, which might have varied across the case studies, as well as through time and spatially in each. This reflects the scarcity of detailed and extended records of avulsion histories of persistently pristine coastal-plain river systems on which to perform a study of this type. Known artificial diversions (and resulting channels) are not treated as avulsions (or products thereof), but a detailed record of human intervention may be lacking for the earliest times of river histories. The only forms of quantification of avulsion frequency that are potentially precise are those based on the number of avulsion events; yet these are unlikely to be accurate in practice due to the fragmentary nature of historical records, especially over millennial timescales. The adoption of the number of channel threads as a proxy for avulsion frequency is subject to several notable problems. The number of channel threads could include a count of palaeochannels whose inception was related to artificial diversions that were not documented as such. The same number fails to quantify re-occupational avulsion events (i.e., the avulsive reoccupation of previously abandoned reaches; Aslan et al., 2005; Reitz et al., 2010; Stouthamer et al., 2011; Reitz and Jerolmack, 2012). It may also include examples of distributary channels whose inception was not due to avulsion, such as for example groundwater-fed channels, or distributary channels that originated from bifurcations around mouth bars (Edmonds and Slingerland, 2007; Hoyal and Sheets, 2009). It also considers particular forms of avulsion ‘by annexation’ (sensu Slingerland and Smith, 2004), such as where groundwater-fed tributaries propagate upstream to intersect other channel reaches, or where tidal channels extend updip to achieve connection with fluvial drainage (cf. Mulrennan and Woodroffe, 1998). The number of delta lobes may underestimate avulsion frequency significantly, as the distinction of delta lobes may depend on the amount of lateral offset of a river and its mouth, which is controlled in part by the variable rates of accommodation generation in the nearshore (e.g., Restrepo and Cantera, 2013). Additionally, the term ‘delta lobe’ may be applied to parts of deltas that themselves are known to have experienced multiple avulsions (e.g., Kazanci and Gulbabazadeh, 2013) or to have been traversed by multiple (palaeo)channels (e.g., Karymbalis et al., 2018; Dong, 2020). Also, the timing of lobe development may be offset relative to the timing of creation of its feeder channel, as lobe growth may be related to variations in the partitioning of discharge and sediment load across multiple distributaries (cf. Vespereanu-Stroe et al., 2017a).

Data on the relative timing of avulsion events of known location, or of the inception of palaeochannels of known location, are not recorded, since these facts are only known for few examples (e.g., Stouthamer et al., 2011; Somoza and Rodríguez-Santalla, 2014). This limits the types of analyses that can be undertaken with the current dataset.

Some river-system variables (bankfull hydraulic geometry, backwater length) represent estimations based on proxy datasets. The variables that characterize the river systems may only reflect present-day or recent conditions; these may not approximate those of pristine natural states, and/or are unlikely to be representative of the entire Holocene timespan over which avulsion metrics have been determined.

The selected case studies are not representative of all types of channel networks seen in coastal-plain river systems. In particular, a bias is likely to exist because studies of avulsion dynamics may focus preferentially on markedly avulsive river systems. Examples for which avulsions are undocumented in the Holocene record (e.g., Mekong, Tamura et al., 2012; Yangtze, Chen and Stanley, 1995) have necessarily been excluded.

The dataset is heterogeneous in terms of the size of the considered study areas relative to the coastal domain. In some cases, the apex of a delta can be identified on the basis of the recognition of topographic

slope breaks, alluvial-valley outlets or persistent avulsion nodes (cf. Stouthamer and Berendsen, 2000; Syvitski et al., 2013; Nooren et al., 2017); in these cases, the extent of the delta sets the size of the study area, provided that the spatial coverage of avulsion-proxy data extends to the delta apex. In the absence of delta apices, the selection of an upstream boundary for areas of interest is necessarily somewhat arbitrary, and placed in such way that the study areas may extend beyond present-day coastal regions. The study areas outline portions of the river systems that have developed relatively near the shoreline at some point in time, but which may now occur far upstream of the coast, where avulsion dynamics may differ. By taking this approach, avulsion events that have occurred in these settings are included in the study. Defining study areas dynamically, so as to track the regressive evolution of the systems, would enable improved analyses; however, this approach is rendered difficult in practice by the limited temporal resolution of avulsion events and palaeoshoreline positions.

### 2.5. Statistical analyses

An assessment is made of relationships between the different avulsion-frequency proxies, between avulsion metrics and the temporal and spatial scales over which they have been determined, and between avulsion metrics and variables describing properties of the river system that are known to reflect its scale. The sign and magnitude of correlations have been quantified by Pearson or Spearman correlation coefficients of the variables or by Pearson correlation coefficients of their corresponding logarithmic transformations. *t*-tests and Welch's one-way ANOVA have been applied to assess statistical significance of differences in mean values of variables across two or more groups of observations, respectively. Normality in data distributions has been tested by Shapiro-Wilk tests. Logarithmic variable transformations have been applied to account for deviations from normality and homoscedasticity in data distributions, to ensure that the assumptions for the use of parametric statistical tests are met; *t*-tests and ANOVA have been applied to log-transformed variables where needed. Statistical significance of both correlations and statistical tests is quantified by *p*-values; outcomes are stated as significant for  $\alpha = 0.05$ . Datasets that are considered as representing relatively complete records of avulsion histories (Table 1), based on what is reported in the data sources and on critical analysis of the broader literature on the same case studies, are labelled as being of 'higher quality'; these are considered separately from the entire data pools in some of the analyses.

## 3. Results

### 3.1. Avulsion metrics and data quality

Some differences are seen in the distributions of avulsion metrics across classes of data quality that reflect the completeness of the associated records (Table 1); yet, these differences are not systematic across the three alternative avulsion-frequency proxies (also termed avulsion 'rates' hereafter for the sake of brevity). Rates based on the number of avulsion events are lower on average for datasets flagged as being of lower quality (Fig. 3a, b). For rates based on counts, mean values are  $34.2 \text{ kyr}^{-1}$  ( $N = 17$ ) and  $2.8 \text{ kyr}^{-1}$  ( $N = 11$ ), and standard deviations are equal to  $101.3 \text{ kyr}^{-1}$  and  $3.2 \text{ kyr}^{-1}$ , for higher and lower-quality datasets respectively; a two-sample *t*-test conducted on log-transformed values of these variables indicates that the difference in mean is statistically significant (*T*-value = 2.15, *p*-value = 0.041, degrees of freedom [d.f.] = 26). For rates normalized by area and river number, mean values are  $0.063 \text{ kyr}^{-1}\text{km}^{-2}$  and  $0.042 \text{ kyr}^{-1}\text{km}^{-2}$ , and standard deviations are  $0.162 \text{ kyr}^{-1}\text{km}^{-2}$  and  $0.104 \text{ kyr}^{-1}\text{km}^{-2}$ , for high and low-quality datasets respectively; however, a two-sample *t*-test on log-transformed values of these variables indicates that mean values do not vary significantly (*T* = 1.51, *p* = 0.152, d.f. = 26). Low- and high-quality avulsion-event datasets cover temporal durations that are on average 2.78 kyr

and 2.85 kyr, respectively. Rates based on the number of channel threads, instead, are lower on average for datasets classified as 'higher quality' (Fig. 3c, d). For rates based on counts, mean values are  $14.3 \text{ kyr}^{-1}$  ( $N = 50$ ) and  $32.2 \text{ kyr}^{-1}$  ( $N = 4$ ), and standard deviations are equal to  $25.1 \text{ kyr}^{-1}$  and  $42.5 \text{ kyr}^{-1}$ , for high and low-quality datasets respectively; the difference in mean values is not statistically significant (two-sample *t*-test of log-transformed values: *T* =  $-1.69$ , *p* = 0.098, d.f. = 52). Corresponding rates normalized by area and river number have mean values of  $0.077 \text{ kyr}^{-1}\text{km}^{-2}$  and  $0.156 \text{ kyr}^{-1}\text{km}^{-2}$ , and standard deviations of  $0.193 \text{ kyr}^{-1}\text{km}^{-2}$  and  $0.311 \text{ kyr}^{-1}\text{km}^{-2}$ , for high and low-quality datasets respectively; the difference in mean values is not statistically significant (two-sample *t*-test of log-transformed values *T* = 0.31, *p* = 0.760, d.f. = 52). Low- and high-quality channel-thread datasets cover on average 2.81 kyr and 3.38 kyr, respectively. Rates based on delta-lobe counts are higher on average for higher-quality datasets, only for rates that are not normalized (Fig. 3e): mean values of these rates are  $7.26 \text{ kyr}^{-1}$  ( $N = 16$ ) and  $4.14 \text{ kyr}^{-1}$  ( $N = 9$ ), and standard deviations are equal to  $17.51 \text{ kyr}^{-1}$  and  $6.68 \text{ kyr}^{-1}$ , for high and low-quality datasets respectively; the difference in mean values is not statistically significant (two-sample *t*-test of log-transformed values: *T* = 1.02, *p* = 0.317, d.f. = 23). Instead, corresponding rates normalized by area and river number (Fig. 3f) have mean values of  $0.017 \text{ kyr}^{-1}\text{km}^{-2}$  and  $0.073 \text{ kyr}^{-1}\text{km}^{-2}$ , and standard deviations of  $0.027 \text{ kyr}^{-1}\text{km}^{-2}$  and  $0.156 \text{ kyr}^{-1}\text{km}^{-2}$ , for high and low-quality datasets respectively; again, means do not differ significantly (two-sample *t*-test of log-transformed values *T* = 0.54, *p* = 0.493, d.f. = 23). Low- and high-quality delta-lobe datasets have average time windows of 4.02 kyr and 3.60 kyr, respectively.

### 3.2. Relationships between avulsion-frequency proxies

Relationships between the three alternative avulsion metrics have been determined to assess the consistency with which they may quantify avulsion frequency and act as proxies for each other. All avulsion metrics are considered as (i) counts per unit time, and as corresponding counts normalized (ii) by area and (iii) by area and number of river systems; hence, nine avulsion metrics are considered overall. The data are presented in Fig. 4, and correlations are reported in Table 2. Positive and statistically significant correlations are seen between any pair of the three metrics having the same form of normalization, or between their log-transformed equivalent (Fig. 4, Table 2). In general, as expected, river systems for which more frequent avulsion events are recorded tend to be associated with larger numbers of delta lobes and channel threads per unit time; the numbers of channel threads and delta lobes per unit time also tend to correlate positively.

### 3.3. Avulsion metrics and spatial scales

Relationships between the alternative avulsion metrics and the size of the study area over which these metrics have been computed have been determined. This analysis provides an assessment of whether the density of avulsion events in coastal-plain river systems varies as a function of spatial scale, on the assumption that the size of the study area is directly proportional to the size of the drainage network that can experience avulsion events. In turn, the results of this analysis can help establish the way in which these metrics can be applied to compare the avulsion histories of different river systems and to study controls on river avulsion. The data are presented in Fig. 5, and correlations are reported in Table 3. If the spatio-temporal density of avulsion events was independent of river-system size, we would expect some positive correlation between non-normalized avulsion metrics and study-area sizes. On the contrary, however, no significant correlations are seen between study-area size and the numbers per unit time of avulsions, channel threads, or delta lobes, or between their log-transformed equivalents. In view of this, necessarily, negative correlations emerge between the size of the study areas and normalized rates, since these rates are computed

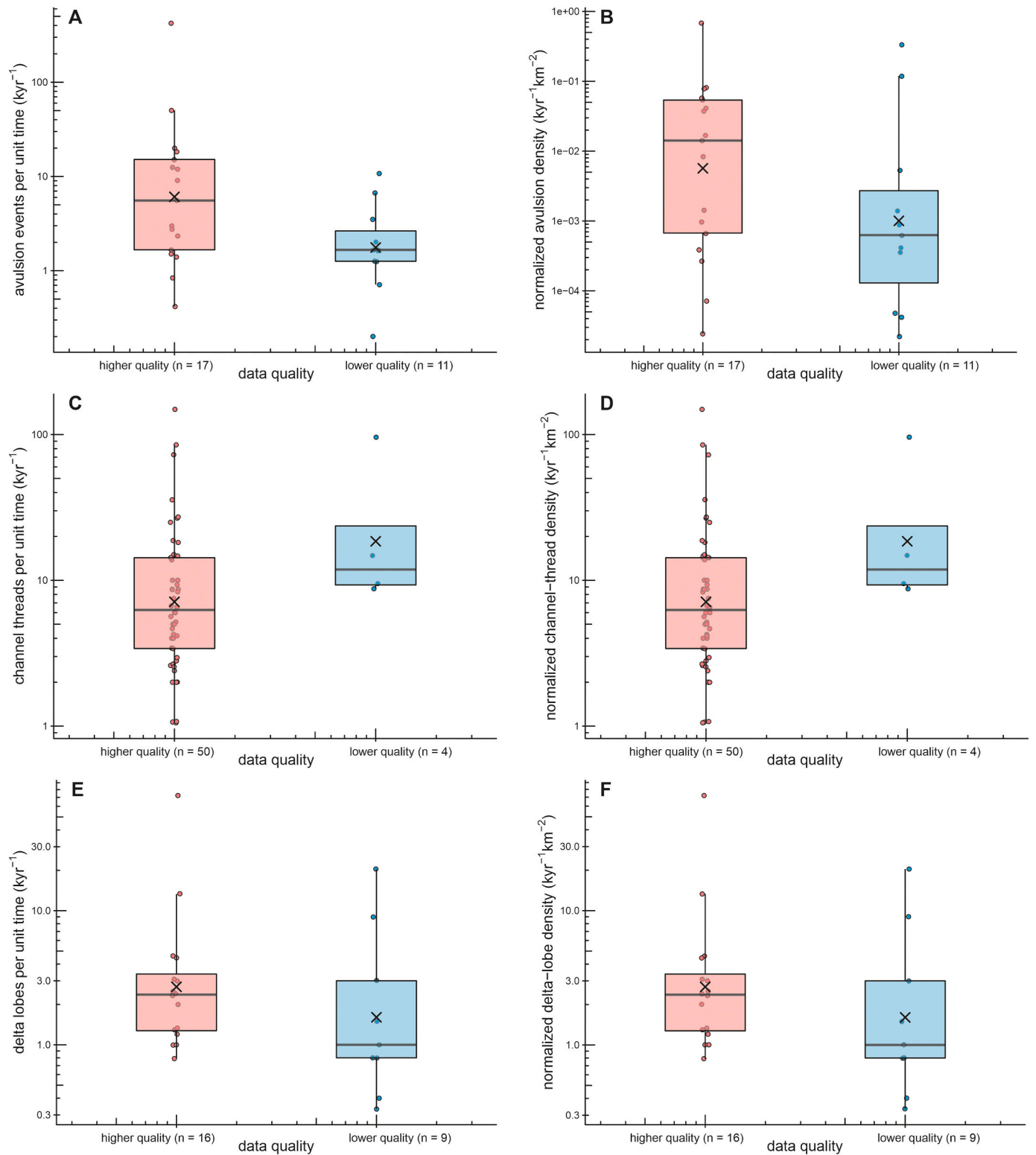


**Fig. 3.** Distributions in avulsion metrics across case studies grouped by data quality, for: number of avulsion events per unit time (A), and corresponding rates normalized by area and river number (B); number of channel threads per unit time (C), and corresponding rates normalized by area and river number (D); number of delta lobes per unit time (E), and corresponding rates normalized by area and river number (F). Spots represent individual examples. Boxplots report interquartile ranges as boxes, mean values as crosses and median values as bars.

with the study-area size as denominator. Negative correlations between log-transformed study-area size and normalized rates are statistically significant. In general, the spatio-temporal densities of avulsion events, channel threads and delta lobes appear to vary with the size of the study

area; conversely, avulsion-frequency proxies do not increase systematically as a function of the size of the area being studied.

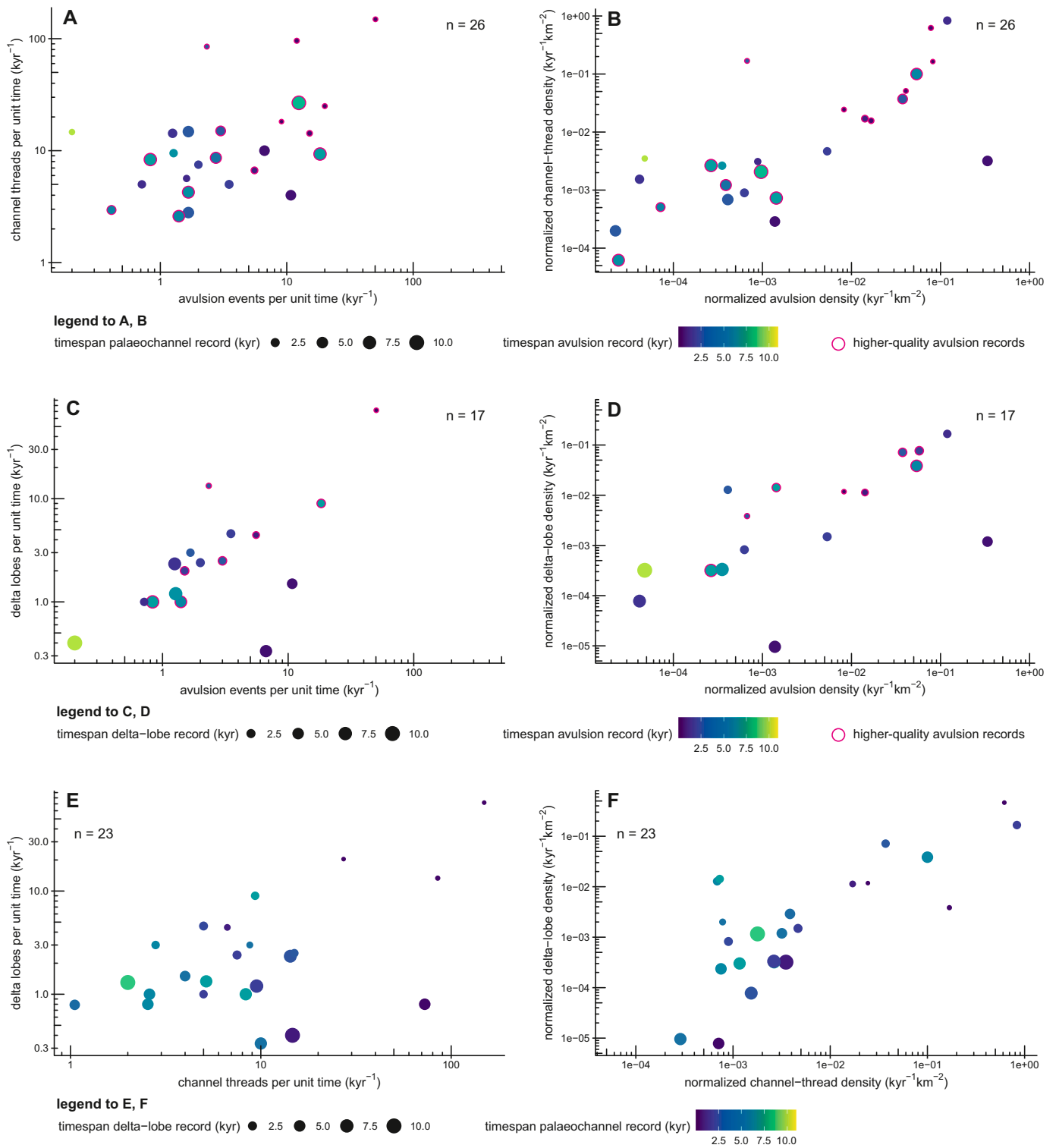


**Fig. 4.** Scatterplots showing relationships between alternative avulsion-frequency metrics: number of channel threads per unit time vs number of avulsion events per unit time (A), and corresponding rates normalized by area and river number (B); number of delta lobes per unit time vs number of avulsion events per unit time (C), and corresponding rates normalized by area and river number (D); number of delta lobes per unit time vs number of channel threads per unit time (E), and corresponding rates normalized by area and river number (F). The size and colour of the spots indicate the timescale over which the avulsion metrics shown in ordinate and abscissa, respectively, have been computed. Higher-quality records of numbers of avulsion events are indicated with magenta circles (see Table 1).

**Table 2**

Pearson correlation coefficients (R) and *p*-values quantifying relationships between the alternative avulsion-frequency metrics, based on different types of normalization, and separately presented for the entire dataset and data from higher-quality records (see Table 1). 'A' indicates rates based on number of avulsion events per unit time; 'C' indicates rates based on number of channel threads per unit time; 'L' indicates rates based on number of delta lobes per unit time. Correlations presented in brackets refer to log-transformed variables. 'N' indicates the number of observations.

	Normalization	Higher-quality records only	All dataset
A vs C	none	$R = 0.753, p = 0.002, N = 14$ ( $R = 0.649, p = 0.012$ )	$R = 0.716, p < 0.001, N = 26$ ( $R = 0.505, p = 0.008$ )
	by area	$R = 0.654, p = 0.011, N = 14$ ( $R = 0.803, p = 0.001$ )	$R = 0.312, p = 0.121, N = 26$ ( $R = 0.719, p < 0.001$ )
	by area and river number	$R = 0.626, p = 0.017, N = 14$ ( $R = 0.825, p < 0.001$ )	$R = 0.312, p = 0.121, N = 26$ ( $R = 0.752, p < 0.001$ )
A vs L	none	$R = 0.986, p < 0.001, N = 7$ ( $R = 0.889, p = 0.007$ )	$R = 0.951, p < 0.001, N = 16$ ( $R = 0.727, p = 0.001$ )
	by area	$R = 0.874, p = 0.010, N = 7$ ( $R = 0.949, p = 0.001$ )	$R = 0.966, p < 0.001, N = 16$ ( $R = 0.779, p < 0.001$ )
	by area and river number	$R = 0.874, p = 0.010, N = 7$ ( $R = 0.949, p = 0.001$ )	$R = 0.966, p < 0.001, N = 16$ ( $R = 0.766, p = 0.001$ )
C vs L	none	$R = 0.931, p < 0.001, N = 12$ ( $R = 0.872, p < 0.001$ )	$R = 0.838, p < 0.001, N = 22$ ( $R = 0.542, p = 0.009$ )
	by area	$R = 0.427, p = 0.166, N = 12$ ( $R = 0.810, p = 0.001$ )	$R = 0.797, p < 0.001, N = 22$ ( $R = 0.769, p < 0.001$ )
	by area and river number	$R = 0.266, p = 0.403, N = 12$ ( $R = 0.791, p = 0.002$ )	$R = 0.794, p < 0.001, N = 22$ ( $R = 0.756, p < 0.001$ )

### 3.4. Avulsion metrics and timescales

An assessment is made of relationships that may exist between the alternative avulsion metrics and the length of time over which they have been computed. This provides a quantification of how avulsion-frequency proxies may vary as a function of their associated time window, either because of geological factors whose influence on coastal river avulsion may have changed through the Holocene, or because of the way the data resolution of avulsion histories may decrease going back in time. The outcomes of this analysis can help inform comparisons of avulsion histories of different river systems and assessments of potential controls on river avulsion. The data are presented in Fig. 6, and correlations are reported in Table 4. Negative, moderate to strong correlations are seen between log-transformed values of the different avulsion metrics and the timespan on which they are calculated; these correlations are statistically significant when based on the entire available dataset (Fig. 6, Table 4). In general, data relating to shorter time windows tend to yield larger values in the different proxies for avulsion frequency.

When considering relationships between avulsion-frequency metrics and timescale, in view of the results presented earlier (Fig. 5, Table 3), it is useful to determine the possible covariance of temporal and spatial scales of the considered samples. This may arise, for example, because the full extent of each study area reflects in part the amount of shoreline progradation that took place during the studied avulsion history, which is itself a function of the time window being considered. However, only weak positive correlations are seen between study-area size and the timespan of each avulsion metric (for log-transformed data; avulsion events: Pearson  $R = 0.292, p = 0.176$ ; channel threads:  $R = 0.286, p = 0.03$ ; delta lobes:  $R = 0.262, p = 0.206$ ).

### 3.5. Avulsion metrics and river-system scale

An assessment is made of relationships that may exist between avulsion metrics and the size of the river systems, and which may arise because of natural controls on avulsion frequency that are inherently related to scale. Particular consideration is given to attributes of the river system that are known to scale to its size and to act as potential controls on avulsion dynamics: the longstream gradient, the shoreline progradation rate, and the backwater length. The gradient advantages that drive channel avulsion may be expected to be more readily generated by channel-ridge aggradation on alluvial plains where the longitudinal gradient is lower (Slingerland and Smith, 2004), since a stronger

contrast between cross-stream and longstream gradients is generated for the same amount of aggradation. Where the river mouth progrades more rapidly, a faster lengthening of the longitudinal profile of the river is associated with a more rapid decrease in longstream gradient, and is expected to be paralleled by faster streambed aggradation; this can again favour the superelevation of channels and the generation of gradient advantages (Jones and Schumm, 1999; Swenson, 2005). Also, avulsion nodes may be expected to be preferentially concentrated near the upstream end of the backwater zone (cf. Chatanantavet et al., 2012); hence, spatial non-uniformity in the distribution of avulsion sites over the study area may reflect: (i) the size of the backwater zone relative to that of the study area over which avulsion metrics are evaluated; and (ii) the magnitude in downdip shift in the backwater limit associated with shoreline progradation and coastal-plain aggradation. The following additional variables are considered as measures of river-system size: the drainage-basin area, the mean yearly water discharge, and the suspended-sediment load. The data are presented in Figs. 7–9 and Supplementary Figs. S1 and S2; correlations are reported in Fig. 10.

As a preliminary analysis, relationships between the size of the study areas and the size of the river systems are determined for all three avulsion metrics. Positive correlations are seen between log-transformed values of the size of the study areas and the drainage-basin areas of the corresponding river systems (for avulsion events: Pearson  $R = 0.784, p < 0.001$ ; for channel threads:  $R = 0.805, p < 0.001$ ; for delta lobes:  $R = 0.793, p < 0.001$ ). In the studied deltaic systems, the extension of the study area typically corresponds to the size of the delta; these results therefore reflect the intuition that larger rivers build larger deltas. This must be taken into account in the evaluation of the following results, in light of how avulsion metrics are influenced by the spatial scale over which they are computed (Fig. 5, Table 3).

In the selected case studies, as expected, drainage-basin areas correlate inversely with coastal-plain gradients (for log-transformed values: Pearson  $R = -0.799, p < 0.001$ ) and directly with mean annual discharges (for log-transformed values:  $R = 0.837, p < 0.001$ ). No significant relationship is observed between drainage-basin areas and any of the avulsion-frequency metrics based on counts per unit time; moderate negative correlations are seen between the log-transformed values of catchment areas and those of normalized counts per unit time of avulsions ( $R = -0.522, p < 0.001$ ), channel threads ( $R = -0.658, p < 0.001$ ) and delta lobes ( $R = -0.706, p < 0.001$ ) (Fig. 7, Supplementary Fig. S1). A significant, albeit weak, relationship with mean water discharge is seen for the number of channel threads per unit time (for log-transformed values:  $R = 0.308, p = 0.025$ ); no relationship is

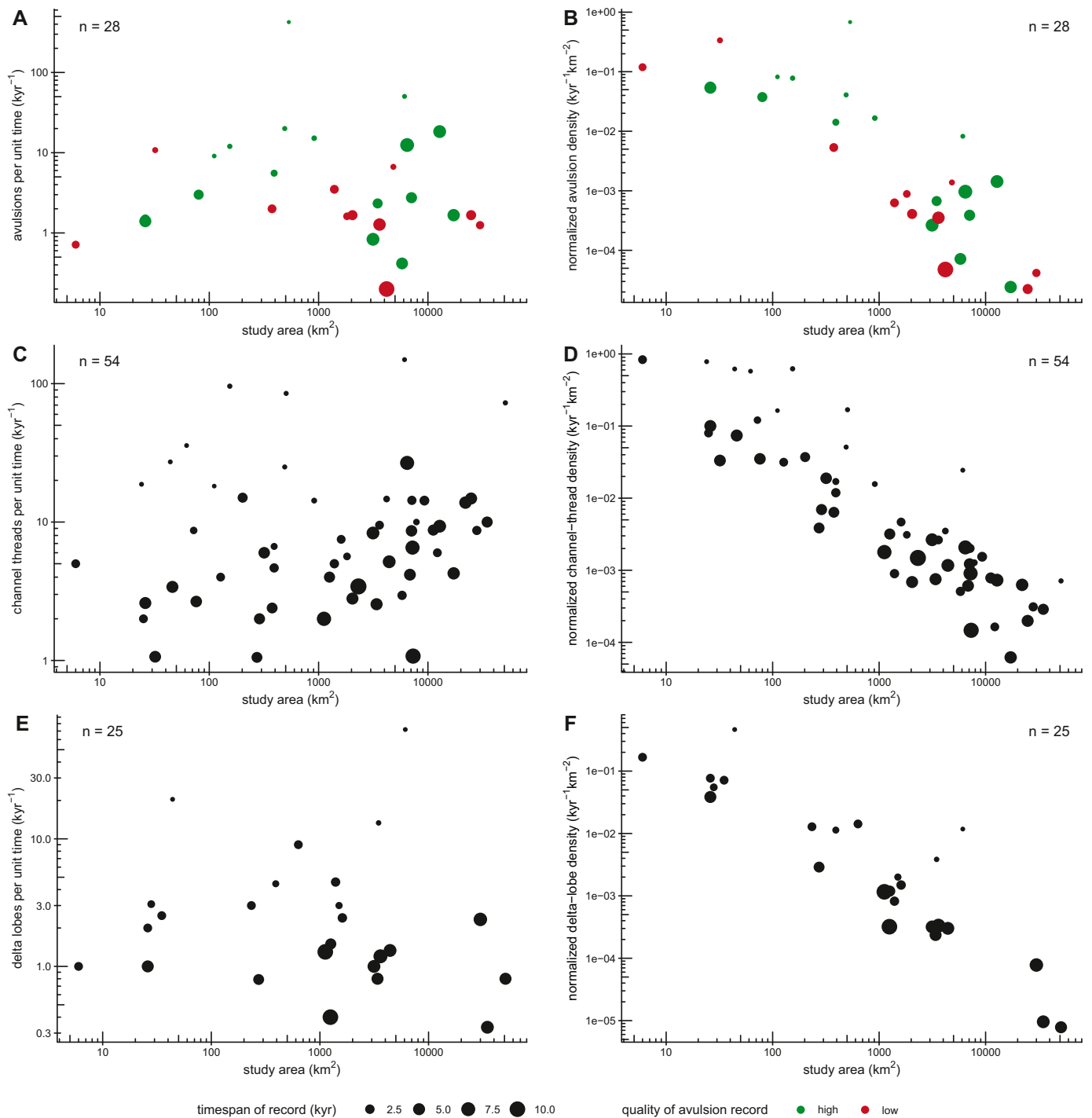


**Fig. 5.** Scatterplots showing relationships between the different avulsion-frequency metrics and the size of the area over which they have been determined, for: number of avulsion events per unit time (A), and corresponding rates normalized by area and river number (B); number of channel threads per unit time (C), and corresponding normalized rates (D); number of delta lobes per unit time (E), and corresponding normalized rates (F). The size of the spots indicates the timescale over which the avulsion metrics have been computed. In A and B, the colour of the spots indicates the quality of the data on number of avulsion events (see Table 1).

seen for corresponding metrics based on avulsion events or delta lobes. Negative relationships are seen between water discharge and normalized metrics based on avulsion events (for log-transformed values:  $R = -0.602$ ,  $p = 0.001$ ), channel threads (for log-transformed values:  $R = -0.613$ ,  $p < 0.001$ ) and delta lobes (for log-transformed values:  $R = -0.769$ ,  $p < 0.001$ ) (Fig. 7, Supplementary Fig. S2). Similarly, a modest but statistically significant negative relationship is seen between the number of channel threads per unit time and the average coastal-plain gradient (for log-transformed values:  $R = -0.341$ ,  $p = 0.012$ ),

whereas no relationship is seen for corresponding rates based on numbers of avulsions or delta lobes (Fig. 7). Positive relationships are seen between the average gradient and normalized metrics based on avulsion events (for log-transformed values:  $R = 0.647$ ,  $p < 0.001$ ), channel threads (for log-transformed values:  $R = 0.532$ ,  $p < 0.001$ ) and delta lobes (for log-transformed values:  $R = 0.598$ ,  $p < 0.001$ ) (Fig. 7).

In the chosen case studies, shoreline progradation rates have been evaluated over different timescales, covering three orders of magnitude. Therefore, these rates may plausibly be affected by the Sadler effect, i.e.,

**Table 3**

Pearson correlation coefficients (R) and *p*-values quantifying relationships between avulsion-frequency metrics and the size of the area over which they have been determined, based on different types of normalization, and separately presented for the entire dataset and data from higher-quality records (see Table 1). 'A' indicates rates based on number of avulsion events per unit time; 'C' indicates rates based on number of channel threads per unit time; 'L' indicates rates based on number of delta lobes per unit time. Correlations presented in brackets refer to log-transformed variables. 'N' indicates the number of observations.

	Normalization	Higher-quality records only	All dataset
A vs area	None	$R = -0.158, p = 0.546, N = 17$ ( $R = 0.020, p = 0.941$ )	$R = -0.120, p = 0.543, N = 28$ ( $R = -0.062, p = 0.756$ )
	by area	$R = -0.277, p = 0.283, N = 17$ ( $R = -0.785, p < 0.001$ )	$R = -0.246, p = 0.207, N = 28$ ( $R = -0.837, p < 0.001$ )
	by area and river number	$R = -0.277, p = 0.282, N = 17$ ( $R = -0.792, p < 0.001$ )	$R = -0.246, p = 0.207, N = 28$ ( $R = -0.839, p < 0.001$ )
C vs area	none	$R = 0.222, p = 0.122, N = 50$ ( $R = 0.203, p = 0.157$ )	$R = 0.158, p = 0.254, N = 54$ ( $R = 0.168, p = 0.224$ )
	by area	$R = -0.228, p = 0.112, N = 50$ ( $R = -0.888, p < 0.001$ )	$R = -0.248, p = 0.071, N = 54$ ( $R = -0.886, p < 0.001$ )
	by area and river number	$R = -0.226, p = 0.115, N = 50$ ( $R = -0.887, p < 0.001$ )	$R = -0.246, p = 0.073, N = 54$ ( $R = -0.887, p < 0.001$ )
L vs area	none	$R = 0.090, p = 0.740, N = 16$ ( $R = 0.264, p = 0.323$ )	$R = -0.060, p = 0.775, N = 25$ ( $R = -0.102, p = 0.626$ )
	by area	$R = -0.287, p = 0.281, N = 16$ ( $R = -0.870, p < 0.001$ )	$R = -0.194, p = 0.354, N = 25$ ( $R = -0.902, p < 0.001$ )
	by area and river number	$R = -0.298, p = 0.262, N = 16$ ( $R = -0.864, p < 0.001$ )	$R = -0.184, p = 0.378, N = 25$ ( $R = -0.901, p < 0.001$ )

by timescale dependency due to the fact that local shoreline accretion is unsteady and the average length of interruptions in sedimentation may increase with the length of time being considered (Sadler, 1981; Sadler and Jerolmack, 2015). Indeed, log-transformed values of progradation rates and the times over which they have been evaluated demonstrate some negative correlation (Pearson  $R = -0.607; p < 0.001$ ). Nevertheless, progradation rates are still more strongly correlated to the rates of sediment supply, through a positive relationship between log-transformed values of progradation rates and total suspended solids in the studied rivers ( $R = 0.675; p < 0.001$ ). In addition, positive relationships are seen between log-transformed values of progradation rates and both catchment size ( $R = 0.577; p < 0.001$ ) and mean annual discharge ( $R = 0.583; p < 0.001$ ). With regard to the avulsion metrics, statistically significant positive correlations are seen between progradation rates and the counts per unit time of both channel threads (for log-transformed values:  $R = 0.760; p < 0.001$ ) and delta lobes (for log-transformed values:  $R = 0.526; p = 0.017$ ); correlation with the number of avulsion events per unit time is also positive, but modest and not significant (for log-transformed values:  $R = 0.303; p = 0.271$ ) (Fig. 8). In spite of positive scaling between progradation rates and study-area sizes (for log-transformed values:  $R = 0.477; p = 0.004; N = 35$ ), no relationships are seen between progradation rates and normalized avulsion metrics (Fig. 8).

Positive correlations are seen between log-transformed values of backwater length and those of both mean annual discharge (Pearson  $R = 0.928, p < 0.001$ ) and catchment area ( $R = 0.883, p < 0.001$ ). These relationships are expected, given how the size of a river's backwater zone is scaled to the size of the river system (cf. Blum et al., 2013): estimations of backwater length used in these analyses are based on ratios between estimated mean bankfull depths and average coastal-plain gradients, and may carry significant error (see Section 2.3).

The dip extent of the backwater zone of each river system ( $L_b$ ) is considered relative to the dip length of the study area ( $l$ ) and the estimated amount of coastal-plain progradation that occurred during the timespan of interest (here termed 'progradation distance';  $D$ ). By assuming, simplistically, that the progradation rate was constant throughout the duration of the characterized avulsion history, the progradation distance is approximated as the product of said rate and the timespan over which each avulsion metric is estimated. Using these quantities, observations are divided into three groups based on (i) whether the dip length of the study area is larger than the backwater length ( $l > L_b$ ), and (ii) on whether the sum of the backwater length and the progradation distance over the timescale of the avulsion metric in

question is larger than the downdip extent of the study area ( $[D + L_b] > l$ ). This grouping is undertaken to attempt discrimination of examples that can be inferred to embody one of the following situations: (i) a backwater limit permanently within the study area ( $[D + L_b] < l$ ); (ii) a backwater limit transitioning from outside to inside the study area ( $[D + L_b] > l$  and  $L_b < l$ ); or (iii) a backwater limit permanently outside of the study area ( $L_b > l$ ). Given the difficulty in constraining values of progradation distance, the dataset associated with each of these groups is, in some cases, very limited in size. Nevertheless, an assessment of differences in the alternative avulsion metrics across the three groups is attempted. Results indicate that values of mean and standard deviation of the avulsion metrics do not vary systematically across the three groups for the three proxies (Table 5). Avulsion-frequency metrics based on numbers of avulsion events are highest on average for examples for which the backwater limit is inferred to have been located outside the study area, and smallest for examples for which the limit is inferred to have been always inside. Metrics based on numbers of channel threads are on average highest for case studies for which the backwater limit is inferred to have transitioned from outside to inside the study area, and smallest for those for which the limit is inferred to have been permanently inside. Metrics based on the number of delta lobes are on average highest for examples for which the backwater limit is inferred to have transitioned inside the study area, and smallest for examples for which the limit is inferred to have been permanently outside. Thus, differences in these metrics are not manifested consistently among the three groups. Furthermore, when tested by means of Welch's one-way ANOVA, the means of the considered avulsion metrics do not differ in a statistically significant manner across the three case-study groups for any of the three avulsion metrics; this may however reflect the small sample sizes (Table 5).

Bivariate analyses indicate that no significant correlations are seen between the estimated backwater length and proxies for avulsion frequency based on the number of avulsion events per unit time (for log-transformed values: Pearson  $R = -0.212, p = 0.332$ ), the number of channel threads per unit time (for log-transformed values:  $R = 0.214, p = 0.145$ ), or the number of delta lobes per unit time (for log-transformed values:  $R = -0.093, p = 0.689$ ) (Fig. 9). As expected, given these results, backwater lengths yield modest to moderate negative correlations with normalized rates based on avulsion events (for log-transformed values:  $R = -0.506, p = 0.014$ ), channel threads (for log-transformed values:  $R = -0.283, p = 0.051$ ), and delta lobes (for log-transformed values:  $R = -0.500, p = 0.021$ ) (Fig. 9); these relationships likely reflect covariance between river-system size, study-area size, and backwater length

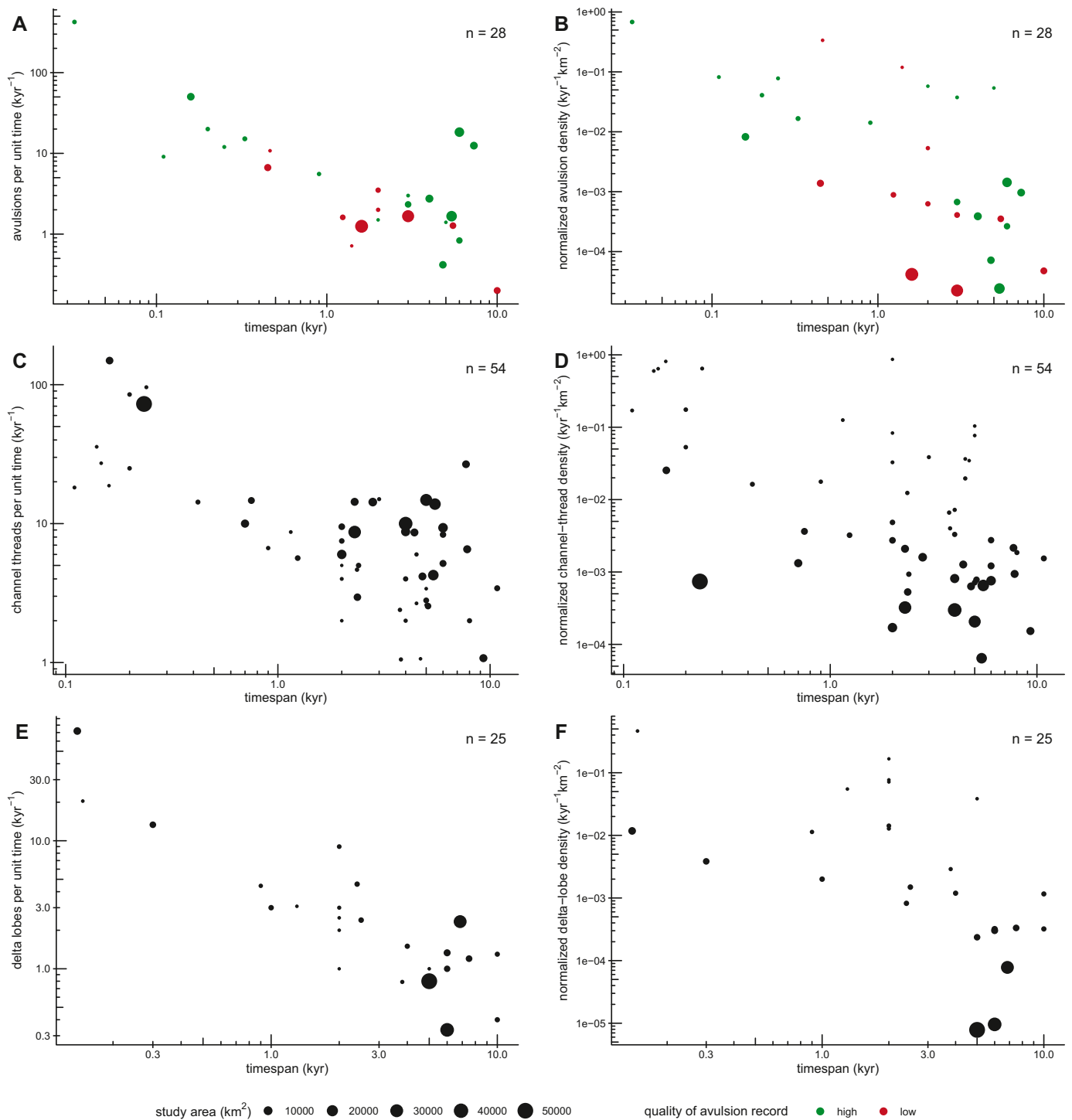


**Fig. 6.** Scatterplots showing relationships between the different avulsion-frequency metrics and the length of time over which they have been determined, for: number of avulsion events per unit time (A), and corresponding rates normalized by area and river number (B); number of channel threads per unit time (C), and corresponding normalized rates (D); number of delta lobes per unit time (E), and corresponding normalized rates (F). The size of the spots indicates the size of the study area over which the avulsion metrics have been computed. In A and B, the colour of the spots indicates the quality of the data on number of avulsion events (see Table 1).

(Fig. 10).

Overall, factors that quantify the size of the river systems tend to exhibit monotonic relationships with normalized proxies for avulsion frequency, due to covariance between these factors and the size of deltas and of the relative study areas on which normalizations are made; these relationships are expressed consistently across the alternative normalized avulsion proxies (Fig. 10). A notable exception to this is observed in

the lack of consistently negative correlations between normalized avulsion metrics and progradation rates, in spite of progradation rates being scaled to the rate of sediment delivery and to catchment size; this reflects the positive correlations between progradation rates and avulsion-frequency metrics that are not normalized by study-area size (Fig. 10).

**Table 4**

Pearson correlation coefficients (R) and *p*-values quantifying relationships between avulsion-frequency metrics and the length of time over which they have been determined, based on different types of normalization, and separately presented for the entire dataset and data from higher-quality records (see Table 1). 'A' indicates rates based on number of avulsion events per unit time; 'C' indicates rates based on number of channel threads per unit time; 'L' indicates rates based on number of delta lobes per unit time. Correlations presented in brackets refer to log-transformed variables. 'N' indicates the number of observations.

	Normalization	Higher-quality records only	All dataset
A vs time	none	$R = -0.331, p = 0.194, N = 17$ ( $R = -0.762, p < 0.001$ )	$R = -0.251, p = 0.198, N = 28$ ( $R = -0.761, p < 0.001$ )
	by area	$R = -0.374, p = 0.139, N = 17$ ( $R = -0.720, p < 0.001$ )	$R = -0.349, p = 0.069, N = 28$ ( $R = -0.668, p < 0.001$ )
	by area and river number	$R = -0.375, p = 0.138, N = 17$ ( $R = -0.719, p < 0.001$ )	$R = -0.349, p = 0.069, N = 28$ ( $R = -0.669, p < 0.001$ )
C vs time	none	$R = -0.400, p = 0.004, N = 50$ ( $R = -0.712, p < 0.001$ )	$R = -0.424, p = 0.001, N = 54$ ( $R = -0.710, p < 0.001$ )
	by area	$R = -0.364, p = 0.009, N = 50$ ( $R = -0.577, p < 0.001$ )	$R = -0.394, p = 0.003, N = 54$ ( $R = -0.609, p < 0.001$ )
	by area and river number	$R = -0.363, p = 0.010, N = 50$ ( $R = 0.565, p < 0.001$ )	$R = -0.393, p = 0.003, N = 54$ ( $R = -0.598, p < 0.001$ )
L vs time	none	$R = -0.398, p = 0.127, N = 16$ ( $R = 0.900, p < 0.001$ )	$R = -0.416, p = 0.039, N = 25$ ( $R = -0.880, p < 0.001$ )
	by area	$R = -0.342, p = 0.194, N = 16$ ( $R = -0.469, p = 0.067$ )	$R = -0.382, p = 0.060, N = 25$ ( $R = -0.606, p = 0.001$ )
	by area and river number	$R = -0.328, p = 0.215, N = 16$ ( $R = -0.469, p = 0.067$ )	$R = -0.365, p = 0.073, N = 25$ ( $R = -0.601, p = 0.001$ )

## 4. Discussion

Here we discuss the significance of the findings presented above by considering how quantifications of river avulsions are affected by the temporal and spatial scales at which they are determined. We then draw practical implications that may be of use to future studies on river avulsion frequency. Before doing this, we must stress that all observed relationships between the studied avulsion metrics and measures of scale exhibit important scatter: this is expected, since the frequency of channel avulsion is controlled by factors whose importance is not systematically dependent on spatial or temporal scales, such as tectonics (e.g., Reitz et al., 2015), presence of compactable peat substrates (van Asselen et al., 2009), and wave- or tide-driven channel stabilization (cf. Swenson, 2005; Rossi et al., 2016), for example.

### 4.1. Avulsion frequency and temporal scales

Relationships between measures quantifying the frequency of river avulsion and the length of time over which those frequencies are extracted (Fig. 6, Table 4) can be explained by both methodological and geological reasons. A methodological explanation lies in the decreasing resolution of historical, sedimentary and geomorphic records with the age of the events, forms or deposits that they document, due to variations in preservation and data granularity. Alternatively, the same trends may be the result of temporal variations in environmental controls through the Holocene. Since the time windows of almost all datasets are anchored to the present day, apparent trends with time scale may actually represent a record of trends in avulsion dynamics through time. These trends could themselves be linked to temporal changes in sediment supply, water discharge, base level, or marine process regime, through their influences on coastal-plain aggradation, shoreline progradation and river hydrodynamics.

Among these factors, the rate of base-level change is perhaps the one that is invoked most commonly as a control on river avulsion, but the way in which relative sea-level changes affect avulsion dynamics is not fully understood. The prevalent view is that the rate of relative sea-level rise may control avulsion frequency by enhancing streambed aggradation, causing the avulsion period to decrease for faster rates of rise (cf. Jerolmack, 2009; Chadwick et al., 2020). Temporal trends in channel-belt avulsion frequency of the Rhine-Meuse delta, for example, have been linked to variations in the rate of sea-level rise accordingly (Stouthamer and Berendsen, 2007; Stouthamer et al., 2011). The negative trends between avulsion-frequency proxies and time length

observed across the considered marginal-marine examples cannot however be explained in terms of a direct relationship between rates of eustatic change and avulsion frequency, given the progressive slowdown in the rate of eustatic sea-level rise through the Holocene (Fleming et al., 1998; Smith et al., 2011; Mörner, 2013; Lambeck et al., 2014). It is nonetheless recognized that avulsions may even become more frequent during slower rates of rise in base level, and that channel super-elevation may even be facilitated by relative sea-level falls in some cases (cf. Nijhuis et al., 2015; Lane et al., 2017). The alternative view that an inverse relationship between avulsion frequency and rates of sea-level rise may emerge is corroborated by results of numerical models, demonstrating how in effect sea-level rise may result in distributed and locally reduced channel aggradation, which can hinder the development of avulsion set-up conditions (Moran et al., 2017). Hence, the possibility that the results of our analyses reflect a global record of variations in rates of eustatic change through the Holocene cannot be discounted.

It is also recognized that avulsion frequency should scale with the rates of shoreline progradation, in light of the control operated by river-mouth lengthening and the associated shift in the river longitudinal profile on streambed aggradation and gradient reduction; this can cause channel super-elevation and the generation of cross-floodplain gradient advantages (Jones and Schumm, 1999; Swenson, 2005; Ratliff et al., 2018). Moreover, channel-mouth progradation can be intimately associated with mouth-bar deposition, which can drive channel aggradation through a morphodynamic backwater effect (Hoyal and Sheets, 2009). However, a tendency of globally increasing shoreline progradation rates through the Holocene, which would explain the results, is at odd with the notion that several of the studied examples have experienced a progressive reduction in sediment supply since the early Holocene (cf. Goodbred Jr and Kuehl, 2000), and with the expected role of autogenic deceleration in progradation during delta growth (Muto and Steel, 1992). The examples used in this study for which time-lapse palaeo-shoreline reconstructions are available show that – when averaged over the timescales of interest – the rates of progradation typically varied to a limited degree and not systematically, demonstrating a progressive deceleration in shoreline progradation through the considered time-spans (e.g., Correggiari et al., 2005b; Fanget et al., 2014; Nooren et al., 2017; Pennington et al., 2017; Zheng et al., 2017; Chen et al., 2020; Nageswara Rao et al., 2020) or only modest acceleration (e.g., Nageswara Rao et al., 2015). It seems therefore unlikely that the observed timescale dependency of avulsion-frequency metrics could reflect temporal variations in progradation rates.

Other natural controls may be at play, such as climate-related factors

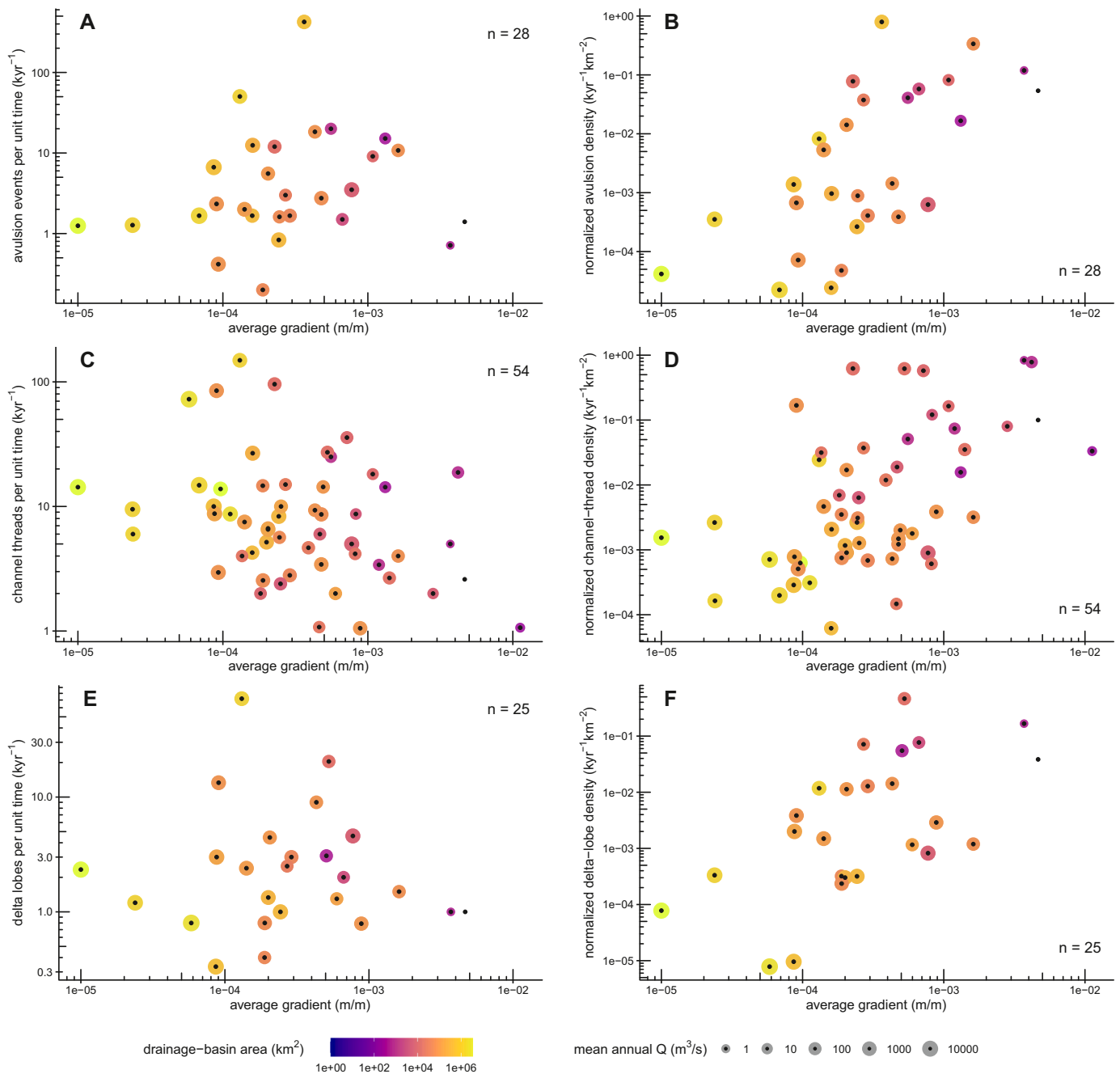


**Fig. 7.** Scatterplots showing relationships between the different avulsion-frequency metrics and the average gradient of the river system over the study area, for: number of avulsion events per unit time (A), and corresponding rates normalized by area and river number (B); number of channel threads per unit time (C), and corresponding normalized rates (D); number of delta lobes per unit time (E), and corresponding normalized rates (F). The size of the spots indicates the mean annual discharge, whereas their colour indicates the drainage-basin area; these two variables are plotted against avulsion-frequency metrics in [Supplementary Figs. S1 and S2](#).

affecting rates of sediment delivery and stream power, which themselves control river mobility. Although it is likely that significant spatial variability in the influence of these factors should mask any global Holocene trend, an assessment of their importance requires separate analyses of their relationships with avulsion-frequency metrics, to be undertaken on examples for which these variables can be constrained.

Anthropogenic factors may also provide a partial explanation of the results. However, a timescale dependency of avulsion frequency is unlikely to be a result of unrecognized human modifications to river drainage networks. Known artificial channel diversions are excluded from our quantifications, and the number of undocumented channel

relocations – which may have been mistreated as avulsions in this study – is expected to increase for more ancient times, which are more likely to lack historical records. It is possible that human engineering of drainage networks could cause water and sediment rerouting in a manner that would affect the avulsion potential of upstream or downstream reaches, but the way in which this could determine temporal trends observed globally cannot be foreseen. Human controls on sediment delivery and water discharge, meanwhile, are known to have varied geographically and through time in both magnitude and direction ([Shi et al., 2002](#); [Oldfield and Dearing, 2003](#); [Erkens et al., 2006](#); [Syvitski and Kettner, 2011](#); [Walling, 2011](#)). An assessment of the possible role of

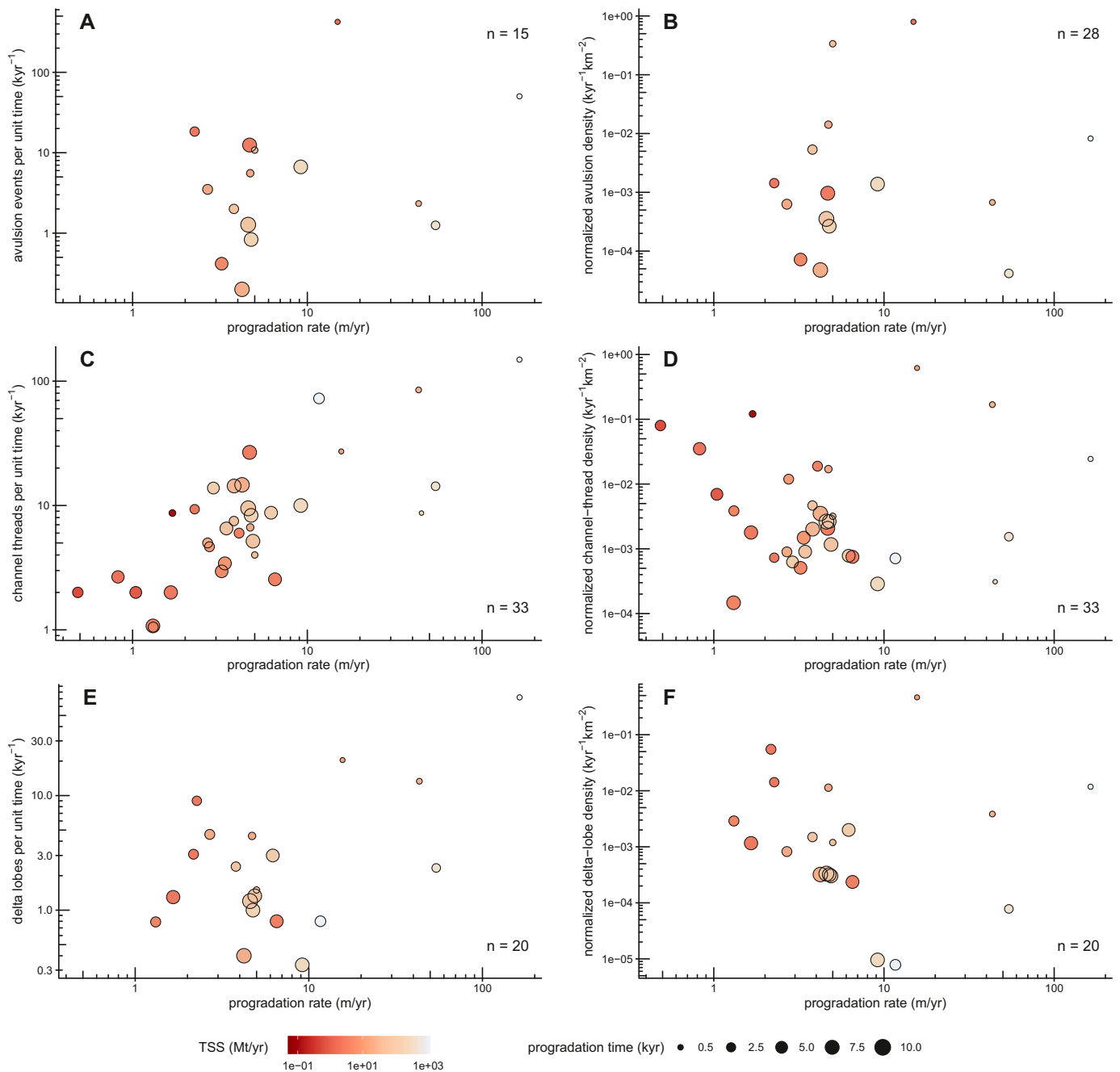


**Fig. 8.** Scatterplots showing relationships between the different avulsion-frequency metrics and the average shoreline progradation rate of the studied coastal plain, for: number of avulsion events per unit time (A), and corresponding rates normalized by area and river number (B); number of channel threads per unit time (C), and corresponding normalized rates (D); number of delta lobes per unit time (E), and corresponding normalized rates (F). The size of the spots indicates the length of time over which the progradation rates have been determined, whereas their colour indicates the total suspended solids (TSS) of the river.

anthropogenic influences on the observed trend requires further analysis, which will rely crucially on the ability to constrain variables describing human pressures on the fluvial systems.

The lack of definitive evidence in support of controls by eustatic sea-level rise, shoreline progradation or human intervention may favour a methodological reason, but a conclusive explanation of the dependency of avulsion-frequency metrics on the time over which they are computed is elusive. To elucidate possible factors affecting the temporal variability in avulsion-frequency metrics, more analysis is needed on datasets including the timing of events, palaeochannel activation, and delta-lobe inception: due to paucity of chronometric constraints, this is in most cases not achievable for the chosen datasets, some of which do not even

afford the establishment of a complete relative chronology.

#### 4.2. Avulsion frequency and spatial scales

Unlike with temporal scales, clear trends between study-area size and avulsion metrics based on simple counts of events, channel threads or delta lobes per unit time do not emerge. There are alternative explanations of the fact that non-normalized avulsion-frequency metrics do not vary with spatial scale, and, implicitly, of the fact that inverse correlations between study-area size and normalized proxies are seen.

These observations may arise from variability in data quality, whereby smaller-scale studies may afford higher resolution in the

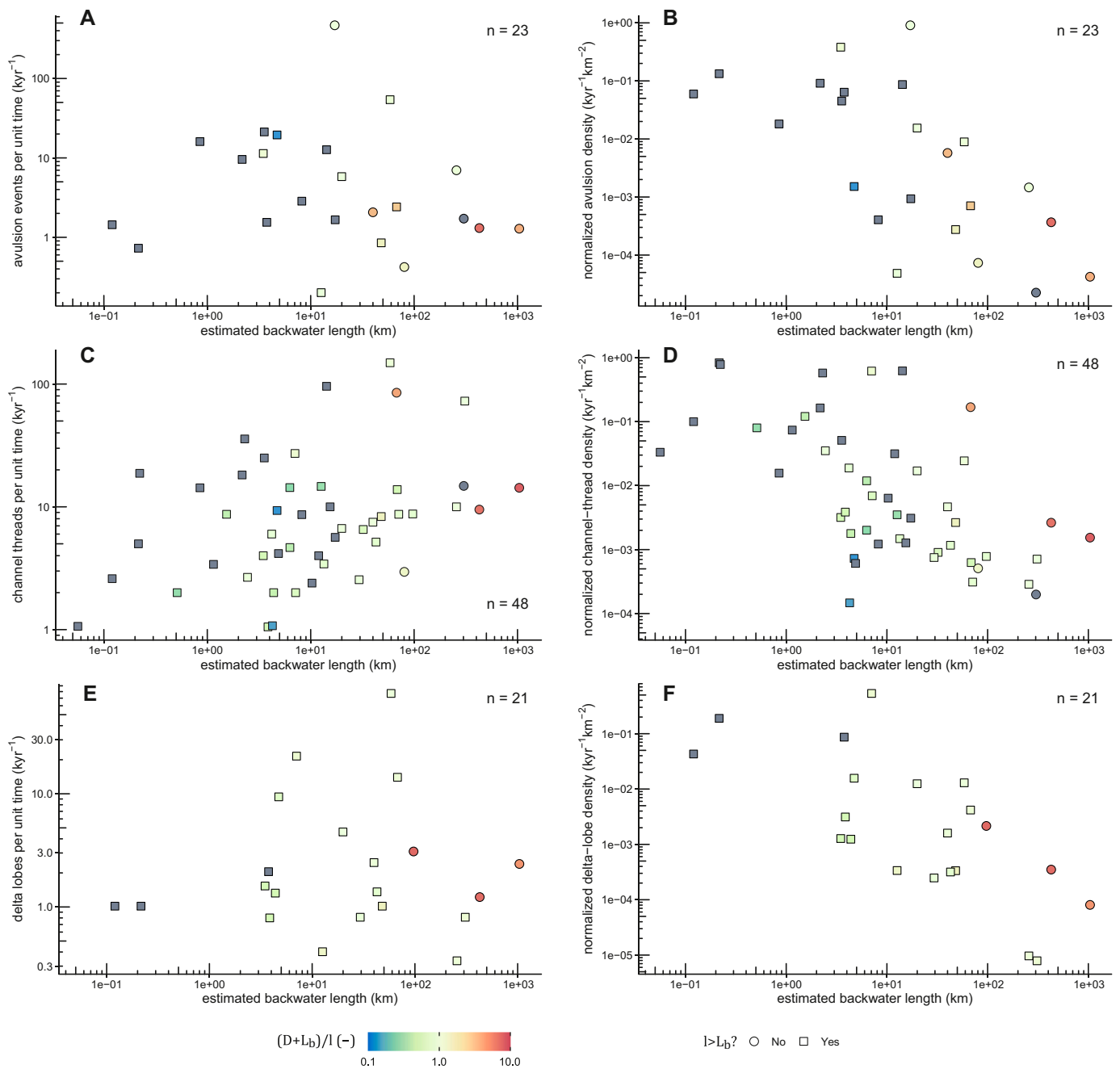


**Fig. 9.** Scatterplots showing relationships between the different avulsion-frequency metrics and the estimated backwater length of the river systems, for: number of avulsion events per unit time (A), and corresponding rates normalized by area and river number (B); number of channel threads per unit time (C), and corresponding normalized rates (D); number of delta lobes per unit time (E), and corresponding normalized rates (F). The shape of the spots indicates whether the downdip extent of the study area ( $l$ ) is larger than the backwater length ( $L_b$ ), whereas their colour reflects a factor equal to the sum of progradation distance (over the timescale of the avulsion metric in question; D) and backwater length divided by the downdip extent of the study area. This ratio is used to discriminate examples that can be inferred to have had (i) a backwater limit permanently within the study area (ratio  $> 1$ ), (ii) a backwater limit transitioning inside the study area (ratio  $< 1$  and  $l > L_b$ ) and (iii) a backwater limit permanently outside of the study area (ratio  $< 1$  and  $l < L_b$ ). Grey symbols indicate examples for which a progradation distance could not be estimated.

definition of avulsion events and drainage networks. We can expect, for example, that a palaeochannel of a certain size that may be mapped on a small fan delta could go unrecognized if occurring on the delta of a large continental-scale river. Nevertheless, based on our classification of datasets on their expected completeness of record, which flags low-quality datasets known as yielding underestimations of avulsion rates, it appears that inherent data variability may not be a major factor in this case. Differences in avulsion-frequency metrics between examples that

are classified as lower versus higher quality are limited in magnitude and not consistent across all proxies (Fig. 3).

It can alternatively be hypothesized that the inverse proportionality between normalized avulsion rates and study-area size reflects possible correlation between study-area size and the timespan of record (e.g., because longer avulsion histories may be associated with more extensive coastal-plain progradation, resulting in larger coastal-plain areas of interest); yet, no significant relationship is seen between these two

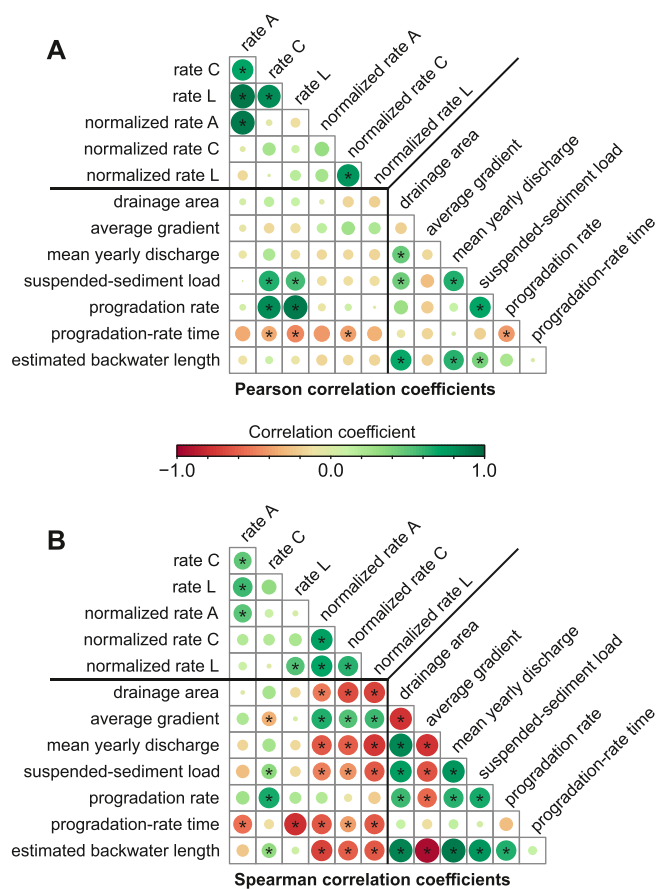


**Fig. 10.** Heatmaps of correlation matrices quantifying correlation between avulsion-frequency metrics and characteristics of the river systems, by means of Pearson (A) and Spearman (B) correlation coefficients; asterisks denote significant correlations ( $p < 0.05$ ). A: avulsion events per unit time; C: channel threads per unit time; L: delta lobes per unit time. Normalized rates are based on normalization by area and river number.

variables.

In view of this, the lack of relationships between the size of the study areas and the magnitude of the avulsion proxies (and, implicitly, the inverse relations between study-area sizes and normalized avulsion proxies) may indicate that smaller coastal river systems tend to record more frequent avulsions relative to the size of their drainage network. One of the objectives of this work was to determine whether the avulsion frequency of a channel network scales with its extent or with quantities that describe river system size, in relation to potential geological controls on river morphodynamics that are known to vary with scale (cf. Powell et al., 2012; Moran et al., 2017). This does not seem to be the

case, overall, if avulsion-frequency proxies that are not normalized are considered. Avulsion metrics based on numbers of events, channel threads or delta lobes do not correlate with explicit measures of river-system size, such as drainage area or mean annual discharge. Correspondingly, normalized avulsion-frequency metrics exhibit negative correlations with the same descriptors of fluvial-system scale, which reflect how the size of the study areas (by which the metrics are normalized) is an indirect measure of the size of the river system.

It is possible that this is observed because of spatial non-stationarity in river avulsions on coastal plains, and this is an explanation that aligns with current understanding of the roles of certain geological controls and autogenic dynamics in determining how avulsions operate through lowland channel networks. In particular, avulsions are commonly clustered around avulsion nodes, which may be preferentially located in the proximity of delta apices, because of controls by backwater effects or basin and floodplain topography (Chatanantavet et al., 2012; Hartley et al., 2017; Ratliff et al., 2021). Conversely, channel avulsions may be relatively less common along more distal reaches subject to streambed erosion due to water-surface drawdown hydrodynamics, operating over areas that are also proportional to river-system size (Chatanantavet et al., 2012; Lamb et al., 2012). If most study areas include persistent nodes where avulsions preferentially occur, like those observed at delta apices, and if the number of nodes in a delta and the associated tempo of nodal avulsion are independent of the size of the river system (with which study areas tend to be scaled), considering a study area that extends further downstream of those nodes may result in a variation in counted features (events, channel threads, delta lobes) that is not proportional to the increase in area. It is recognized for example that the size of delta lobes tends to be scaled to the backwater length (Ganti et al., 2016a; Moodie et al., 2019), and hence to river-system size and to the size of the delta itself; this notion is consistent with the presented quantifications of delta-lobe switching frequency. In relation to the supposed importance of backwater hydrodynamics as a cause for non-stationarity in the location of avulsion occurrence, it is also useful to consider the coverage of the study areas relative to the backwater lengths of their associated rivers. In this work, the spatial variability in avulsion frequency that may be linked to backwater processes is only considered by means of some crude analysis, by considering the size and amount of shift of the backwater zone relative to the size of the study area, as a way to determine whether avulsion-frequency metrics may differ within backwater reaches characterized by non-uniform river flow. Results of this analysis indicate that avulsion rates associated with examples inferred to have had a backwater limit permanently outside of the study area are not systematically lower, which would instead be expected if avulsions were less likely in the downstream portion of the backwater zone (Chatanantavet et al., 2012). It must be recognized, however, that the location at which avulsion nodes may preferentially develop along backwater reaches is not well understood. Current research suggests that this location may not coincide with the upstream portion of the backwater zone, and that it may be determined in part by other factors, such as discharge variability and progradation history

**Table 5**

Variations in mean and standard deviations of avulsion metrics across groups of case studies defined on the basis of the relative extent of backwater length, progradation distance and study-area dip length; statistical significance in the difference between mean values across the three groups is determined by means of Welch's one-way ANOVA applied to log-transformed quantities. L: study-area dip length; L<sub>b</sub>: backwater length; D: progradation distance; SD: standard deviation; A: avulsion events per unit time; C: channel threads per unit time; L: delta lobes per unit time. Normalized rates are based on normalization by area and river number.

	(D + L <sub>b</sub> ) < 1			(D + L <sub>b</sub> ) > 1, L <sub>b</sub> < 1			L <sub>b</sub> > 1			ANOVA
	mean	SD	N	mean	SD	N	mean	SD	N	
Rate A (kyr <sup>-1</sup> )	9.3	9.1	2	14.0	20.7	5	72.6	172.3	6	F[2, 2.63] = 0.10, p = 0.905
Normalized rate A (kyr <sup>-1</sup> km <sup>-2</sup> )	0.74 × 10 <sup>-3</sup>	0.98 × 10 <sup>-3</sup>	2	0.072	0.066	5	0.13	0.32	6	F[2, 3.56] = 0.93, p = 0.473
Rate C (kyr <sup>-1</sup> )	9.2	15.2	21	34.8	56.5	6	27.9	38.3	4	F[2, 6.20] = 2.49, p = 0.160
Normalized rate C (kyr <sup>-1</sup> km <sup>-2</sup> )	0.014	0.031	21	0.111	0.249	6	0.043	0.083	4	F[2, 6.01] = 0.63, p = 0.566
Rate L (kyr <sup>-1</sup> )	2.45	3.22	6	12.78	23.26	9	2.18	0.91	3	F[2, 9.40] = 0.41, p = 0.673
Normalized rate L (kyr <sup>-1</sup> km <sup>-2</sup> )	0.33 × 10 <sup>-2</sup>	0.54 × 10 <sup>-2</sup>	6	0.055	0.153	9	0.80 × 10 <sup>-3</sup>	0.10 × 10 <sup>-2</sup>	3	F[2, 6.65] = 0.55, p = 0.600

(Ganti et al., 2016a, 2016b; Moodie et al., 2019; Brooke et al., 2020; Chadwick et al., 2020). To elucidate how backwater processes may have controlled the avulsion histories of Holocene deltas, additional analysis is needed; this would need to leverage on chronometric constraints for both avulsion sites and palaeoshorelines to allow the determination of avulsion lengths (sensu Ganti et al., 2016b).

The absence of correlation between study-area size and avulsion-frequency metrics may alternatively reflect the fact that smaller rivers are inherently more avulsive – in proportion to the extent of their drainage networks – because of the role of external factors that vary with scale. This idea might clash with current understanding of certain controls on avulsion set-up conditions, notably with the fact that smaller river systems tend to be characterized by steeper streamwise gradients, or by slower river-mouth progradation (Aadland and Helland-Hansen, 2019). Yet, the importance of certain upstream or intrabasinal controls on avulsion triggers and/or preconditions may vary systematically with the scale of the river system. It is possible, for example, that smaller deltas experience floods that are relatively more conducive to channel avulsion, or exhibit substrate characteristics or dominant morphodynamic behaviours that make their channels more susceptible to diversion. It is known for example that rivers with catchments that are on average smaller tend to be characterized by higher variability in daily water discharge within a year, by higher sediment delivery rates in proportion to their discharge, and by suspended-sediment flux concentrated over comparatively shorter durations (Walling, 1983; Meybeck et al., 2003; Hansford et al., 2020). Some of the studied fan deltas with small, high-relief catchments may have been subject to avulsions driven by channel chocking caused by mass flows (cf. Karymbalis et al., 2010). By contrast, the largest, suspended-load-dominated river systems may be characterized by increased fractions of cohesive sediment in levees and overbank areas, which can stabilize channels and inhibit river avulsion (cf. Edmonds and Slingerland, 2010; Caldwell and Edmonds, 2014). Additionally, in the chosen dataset, several of the smaller river systems tend to be associated with catchments and basins located in tectonically active areas (e.g., river systems of Greece, Taiwan, Philippines), where the influence of seismic triggers to avulsion (e.g., local surface deformation, levee liquefaction, groundwater expulsion; cf. Quigley and Duffy, 2020) can be expected to be higher. To establish whether our observations are determined by any of these potential controls, further analyses need to be undertaken in which these factors are expressly considered.

On account of the lack of correlation between study-area size and ‘pure’ avulsion frequency metrics, and given the relationships between progradation rates, sediment-supply rates, and river-system size, the observed correlations between progradation rates and avulsion-frequency estimations based on channel-thread or delta-lobe counts may be interpreted to support the view that an increase in avulsion frequency may result from faster shoreline progradation (Jones and Schumm, 1999; Swenson, 2005). More rapid progradation does not correspond to higher spatio-temporal density of avulsion events, but this does not necessarily challenge this interpretation, since the size of a study area reflects the scale of the river system, with which avulsion-density metrics correlate negatively overall. Also, any relationships between avulsion metrics and progradation rates may be obfuscated by how some of the studied systems may have undergone progradation under partially forced regressive conditions (e.g., Kazanci et al., 2004; Nijhuis et al., 2015). Nevertheless, any inference of how rates of channel-mouth progradation and associated drivers may control avulsion frequency is not strongly supported by data on avulsion-event counts. It must also be considered that higher progradation and sediment-supply rates may be linked to enhanced mouth-bar growth, and hence to a larger number of bifurcations around mouth bars, from which some of the mapped palaeochannels may have evolved.

In summary, whether relationships between normalized avulsion-frequency metrics and the scale over which they are determined represent apparent trends due to methodological limitations, or a record of

how the behaviour of avulsive channel networks changes in relation to factors that vary with the scale of the river system, cannot be established with confidence solely on the basis of the presented analyses.

#### 4.3. Practical implications

If we trust that data quality does not have a major effect on the adopted metrics, relationships between measures of avulsion frequency and the size of the study area over which they are determined provide guidance on the application of these metrics for comparisons of different fluvial systems. A hypothesis was made that – to facilitate comparisons between different river systems – rates may need to be normalized by the area over which they have been considered, based on the argument that the size of the study area is proportional to the size of the channel network, such that a larger cumulative length of channel threads that can avulse is sampled. The findings of this work indicate that measures of channel-avulsion frequency may not scale proportionally with the planform extent of the area over which they are evaluated, if the size of that area (e.g., extent of a delta plain) is directly related to the size of the river system. It is also observed that, expectedly, avulsion statistics vary as function of the time window over which they are determined. Hence, quantifications of avulsion frequency or interavulsion period do not seem meaningful in absence of some specification of the temporal and spatial scales over which they have been determined. These considerations should be born in mind when comparing avulsion-frequency proxies of different coastal-plain river systems and over different scales. In attempting to quantify avulsion frequency in a way that enables meaningful comparisons, it is recommended that (i) uncertainties associated with apparent scale dependency are recognized, (ii) alternative integrative approaches are adopted (i.e., simultaneous consideration of raw and normalized avulsion statistics), and (iii) scales of the spatial and temporal samples are explicitly reported.

#### 5. Conclusions

An analysis has been conducted of the avulsion histories of 57 coastal-plain river systems, which have been quantified by means of metrics based on numbers of avulsion events, channel threads and delta lobes; these quantifications have been made with consideration of the size of the study areas and of the number of separate rivers traversing them.

These metrics vary with temporal and spatial scales in ways that may be due to both geological and methodological reasons, such as non-uniformity in the way controlling factors operate in space and time, or variations in the resolution of avulsion records with their temporal and spatial extent. Proxies for coastal-plain river avulsion frequency tend to decrease in magnitude as the time window over which they are evaluated increases, likely because of Holocene trends in the importance of avulsion drivers or due to a decrease in the completeness of older avulsion records. Non-normalized avulsion-frequency metrics are not directly related to the size of the area over which they are determined, indicating that smaller deltas tend to record more frequent avulsions in proportion to the extent of their channel networks. This may be an apparent trend due to variations in resolution with the scale of investigation; it may otherwise represent a true emerging characteristic of river deltas, due to non-stationarity in channel avulsion, or to factors acting as avulsion triggers or enablers whose importance varies in relation with river-system scale (e.g., variability in water and sediment discharge, substrate stability).

Measures of the spatio-temporal density of avulsion events in coastal-plain fluvial systems vary in relation to spatial and temporal scales, and this has implications on how we quantify and compare the avulsion frequency of lowland rivers.

## Data statement

A file containing data employed in this paper is included as supplementary material, along with explanation of the data fields.

## Declaration of Competing Interest

The authors declare that they have no known competing financial interests or personal relationships that could have appeared to influence the work reported in this paper.

## Acknowledgements

We thank the sponsors of the Fluvial, Eolian & Shallow-Marine Research Group for financial support to this research (AkerBP, Areva [now Orano], BHP, Cairn India [Vedanta], Chevron, CNOOC International, ConocoPhillips, Equinor, Murphy Oil, Occidental, Saudi Aramco, Shell, Tullow Oil, Woodside, and YPF). We thank five anonymous reviewers for their comments, which have helped improve this paper.

## Appendix A. Supplementary data

Supplementary data to this article can be found online at <https://doi.org/10.1016/j.earscirev.2022.104043>.

## References

- Aadland, T., Helland-Hansen, W., 2019. Progradation rates measured at modern river outlets: A first-order constraint on the pace of deltaic deposition. *J. Geophys. Res. Earth Surf.* 124 (2), 347–364.
- Abdrasilov, S.A., Tulebaeva, K.A., 1994. Dynamics of the Ili delta with consideration of fluctuations of the level of Lake Balkhash. *Hydrotech. Constr.* 28 (8), 421–426.
- Ainsworth, R.B., Vakarelov, B.K., Eide, C.H., Howell, J.A., Bourget, J., 2019. Linking the high-resolution architecture of modern and ancient wave-dominated deltas: processes, products, and forcing factors. *J. Sediment. Res.* 89 (2), 168–185.
- Akter, J., Sarker, M.H., Popescu, I., Roelvink, D., 2016. Evolution of the Bengal Delta and its prevailing processes. *J. Coast. Res.* 32 (5), 1212–1226.
- Al-Hamad, S.S., Albdran, B.N., Pournelle, J.R., 2017. Geological History of Shatt Al-Arab River, South of Iraq. *Int. J. Sci. Res.* 6 (1), 2029–2039.
- Allison, M.A., Khan, S.R., Goodbred Jr., S.L., Kuehl, S.A., 2003. Stratigraphic evolution of the late Holocene Ganges–Brahmaputra lower delta plain. *Sediment. Geol.* 155 (3–4), 317–342.
- Andreadis, K.M., Schumann, G.J.P., Pavelsky, T., 2013. A simple global river bankfull width and depth database. *Water Resour. Res.* 49 (10), 7164–7168.
- Ashmore, P.E., Day, T.J., 1988. Spatial and temporal patterns of suspended-sediment yield in the Saskatchewan River basin. *Can. J. Earth Sci.* 25 (9), 1450–1463.
- Aslan, A., White, W.A., Warne, A.G., Guevara, E.H., 2003. Holocene evolution of the western Orinoco Delta, Venezuela. *Geol. Soc. Am. Bull.* 115 (4), 479–498.
- Aslan, A., Autin, W.J., Blum, M.D., 2005. Causes of river avulsion: insights from the late Holocene avulsion history of the Mississippi River, USA. *J. Sediment. Res.* 75 (4), 650–664.
- Ataol, M., 2015. A crevasse splay induced avulsion on the Ceyhan delta. *J. Int. Social Res.* 8, 675–681.
- Begg, G.W., 1978. The Estuaries of Natal: A Resource Inventory Report to the Natal Town and Regional Planning Commission (Vol. 41). Natal Town and Regional Planning Commission.
- Berendsen, H.J.A., Stouthamer, E., 2002. Paleogeographic evolution and avulsion history of the Holocene Rhine-Meuse delta, The Netherlands. *Netherlands J. Geosci.* 81 (1), 97–112.
- Bernardes, M.C., Knoppers, B.A., Rezende, C.E., Souza, W.F.L., Ovalle, A.R.C., 2012. Land-sea interface features of four estuaries on the South America Atlantic coast. *Braz. J. Biol.* 72, 761–774.
- Bhattacharya, J.P., Miall, A.D., Ferron, C., Gabriel, J., Randazzo, N., Kynaston, D., Jicha, B.R., Singer, B.S., 2019. Time-stratigraphy in point sourced river deltas: application to sediment budgets, shelf construction, and paleo-storm records. *Earth Sci. Rev.* 199, 102985.
- Blum, M., Martin, J., Milliken, K., Garvin, M., 2013. Paleovalley systems: insights from Quaternary analogs and experiments. *Earth Sci. Rev.* 116, 128–169.
- Bondesan, M., Favero, V., Viñals, M.J., 1995. New evidence on the evolution of the Po-delta coastal plain during the Holocene. *Quat. Int.* 29, 105–110.
- Brooke, S.A., Ganti, V., Chadwick, A.J., Lamb, M.P., 2020. Flood variability determines the location of Lobe-Scale Avulsions on Deltas: Madagascar. *Geophys. Res. Lett.* 47, e2020GL088797.
- Bryant, M., Falk, P., Paola, C., 1995. Experimental study of avulsion frequency and rate of deposition. *Geology* 23 (4), 365–368.
- Caldwell, R.L., Edmonds, D.A., 2014. The effects of sediment properties on deltaic processes and morphologies: a numerical modeling study. *J. Geophys. Res. Earth Surf.* 119 (5), 961–982.
- Chadwick, A.J., Lamb, M.P., Ganti, V., 2020. Accelerated river avulsion frequency on lowland deltas due to sea-level rise. *Proc. Natl. Acad. Sci.* 117 (30), 17584–17590.
- Chamberlain, E.L., Törnqvist, T.E., Shen, Z., Mauz, B., Wallinga, J., 2018. Anatomy of Mississippi Delta growth and its implications for coastal restoration. *Sci. Adv.* 4 (4), eaar4740.
- Chang, J.C., Chen, H.L., 2001. Geomorphological changes on coastal plain in southwestern Taiwan. *Western Pacific Earth Sci.* 1 (1), 107–114.
- Chatanantavet, P., Lamb, M.P., Nittrouer, J.A., 2012. Backwater controls of avulsion location on deltas. *Geophys. Res. Lett.* 39 (1), L01402.
- Chen, Z., Stanley, D.J., 1995. Quaternary subsidence and river channel migration in the Yangtze delta plain, eastern China. *J. Coast. Res.* 11, 927–945.
- Chen, D., Li, X., Saito, Y., Liu, J.P., Duan, Y., Zhang, L., 2020. Recent evolution of the Irrawaddy (Ayeyarwady) Delta and the impacts of anthropogenic activities: A review and remote sensing survey. *Geomorphology* 365, 107231.
- Cheng, L., Xu, Q., Guo, H., Li, M., Yang, N., Liu, J., Zhao, J., Guo, J., 2020. The Late Holocene stratum and evolution in the Luanhe River Delta. *Quat. Sci.* 40 (3), 751–763.
- Cohen, S., Kettner, A.J., Syvitski, J.P., Fekete, B.M., 2013. WBMsed, a distributed global-scale riverine sediment flux model: model description and validation. *Comput. Geosci.* 53, 80–93.
- Colombera, L., Bersezio, R., 2011. Impact of the magnitude and frequency of debris-flow events on the evolution of an alpine alluvial fan during the last two centuries: responses to natural and anthropogenic controls. *Earth Surf. Process. Landf.* 36 (12), 1632–1646.
- Colombera, L., Mountney, N.P., 2020. On the geological significance of clastic parasequences. *Earth Sci. Rev.* 201, 103062.
- Correggiari, A., Cattaneo, A., Trincardi, F., 2005a. Depositional patterns in the late Holocene Po delta system. In: Giosan, L., Bhattacharya, J.P. (Eds.), *River Deltas—Concepts, Models, and Examples*, 83. SEPM Special Publication, pp. 13–30.
- Correggiari, A., Cattaneo, A., Trincardi, F., 2005b. The modern Po Delta system: lobe switching and asymmetric prodelta growth. *Mar. Geol.* 222, 49–74.
- Cuong, T.Q., 2009. Soil properties, topography and Quaternary substratum in the edge of the Red River delta, Vietnam. Doctoral Dissertation. University of Natural Resources and Applied Life Sciences, Vienna.
- Da Rocha, T.B., 2013. A planície costeira meridional do complexo deltáico do rio Paraíba do Sul (RJ): arquitetura deposicional e evolução do paisagem durante o Quaternário Tardio. Doctoral Dissertation. Universidade Federal do Rio de Janeiro.
- Dash, C., Jaiswal, M.K., Pati, P., Patel, N.K., Singh, A.K., Shah, R.A., 2020. Fluvial response to Late Quaternary sea level changes along the Mahanadi delta, east coast of India. *Quat. Int.* 553, 60–72.
- Deom, J.M., Sala, R., Laudisoit, A., 2019. The Ili River Delta: Holocene Hydrogeological Evolution and Human Colonization. In: Yang, L.E., Bork, H.R., Fang, X., Mischke, S. (Eds.), *Socio-Environmental Dynamics along the Historical Silk Road*. Springer, Cham, pp. 67–94.
- Dinis, P.A., Huvi, J., Callapez, P.M., 2018. The Catumbela delta (SW Angola). Processes determining a history of changing asymmetry. *J. Afr. Earth Sci.* 145, 68–79.
- Dominguez, J.M.L., Bittencourt, A.C.S.P., Martin, L., 1981. Esquema evolutivo da sedimentação quaternária nas feições deltaicas dos rios São Francisco (SE/AL), Jequitinhonha (BA), Doce (ES) e Paraíba do Sul (RJ). *Rev. Brasil. Geociê.* 11 (4), 227–237.
- Donaldson, A.C., Martin, R.H., Kanes, W.H., 1970. Holocene Guadalupe delta of Texas gulf coast. In: Morgan, J.P. (Ed.), *Deltaic Sedimentation Modern and Ancient*, 15. SEPM Special Publication, pp. 107–137.
- Dong, T.Y., 2020. Dynamics of delta building across different scales as informed by the Selenga River Delta, Russia. Doctoral dissertation. Rice University, Houston.
- Duskayev, K., Myrzakhmetov, A., Zhanabayeva, Z., Klein, I., 2020. Features of the Sediment Runoff Regime Downstream the Ile River. *J. Ecol. Eng.* 21 (2), 117–125.
- Edmonds, D.A., Slingerland, R.L., 2007. Mechanics of river mouth bar formation: Implications for the morphodynamics of delta distributary networks. *J. Geophys. Res. Earth Surf.* 112, F02034.
- Edmonds, D.A., Slingerland, R.L., 2010. Significant effect of sediment cohesion on delta morphology. *Nat. Geosci.* 3 (2), 105–109.
- Efstratiadis, A., Tegos, A., Varveris, A., Koutsoyiannis, D., 2014. Assessment of environmental flows under limited data availability: case study of the Acheloos River, Greece. *Hydrol. Sci. J.* 59 (3–4), 731–750.
- El Bastawesy, M., Cherif, O.H., Sultan, M., 2017. The geomorphological evidences of subsidence in the Nile Delta: Analysis of high resolution topographic DEM and multi-temporal satellite images. *J. Afr. Earth Sci.* 136, 252–261.
- El Bastawesy, M., Gebremichael, E., Sultan, M., Attwa, M., Sahnour, H., 2020. Tracing Holocene channels and landforms of the Nile Delta through integration of early elevation, geophysical, and sediment core data. *The Holocene* 30 (8), 1129–1141.
- Erkens, G., Cohen, K.M., Gouw, M.J., Middelkoop, H., Hoek, W.Z., 2006. Holocene sediment budgets of the Rhine Delta (The Netherlands): a record of changing sediment delivery. In: *Sediment Dynamics and the Hydromorphology of Fluvial Systems*, Proceedings. Dundee, pp. 406–415.
- Erol, O., 2003. Geomorphological evolution of the Ceyhan River delta: Eastern Mediterranean coast of Turkey. *Aegean Geograph. J.* 12 (2), 59–81.
- Fanget, A.S., Berné, S., Jouet, G., Bassetti, M.A., Dennielou, B., Maillat, G.M., Tondut, M., 2014. Impact of relative sea level and rapid climate changes on the architecture and lithofacies of the Holocene Rhone subaqueous delta (Western Mediterranean Sea). *Sediment. Geol.* 305, 35–53.
- Field, J., 2001. Channel avulsion on alluvial fans in southern Arizona. *Geomorphology* 37 (1–2), 93–104.
- Fielding, C.R., Trueman, J.D., Alexander, J., 2005a. Sharp-based, flood-dominated mouth bar sands from the Burdekin River Delta of northeastern Australia: extending

- the spectrum of mouth-bar facies, geometry, and stacking patterns. *J. Sediment. Res.* 75 (1), 55–66.
- Fielding, C.R., Trueman, J., Alexander, J., 2005b. Sedimentology of the modern and Holocene Burdekin River Delta of north Queensland, Australia—controlled by river output, not by waves and tides. In: Giosan, L., Bhattacharya, J. (Eds.), *River Deltas: Concepts, Models and Examples*, 83. SEPM, Special Publication, pp. 467–496.
- Fielding, C.R., Trueman, J.D., Alexander, J., 2006. Holocene depositional history of the Burdekin River Delta of northeastern Australia: a model for a low-accommodation, highstand delta. *J. Sediment. Res.* 76 (3), 411–428.
- Fleming, K., Johnston, P., Zwart, D., Yokoyama, Y., Lambeck, K., Chappell, J., 1998. Refining the eustatic sea-level curve since the Last Glacial Maximum using far-and intermediate-field sites. *Earth Planet. Sci. Lett.* 163 (1–4), 327–342.
- Funabiki, A., Saito, Y., Phai, V.V., Nguyen, H., Haruyama, S., 2012. Natural levees and human settlement in the Song Hong (Red River) delta, northern Vietnam. *The Holocene* 22 (6), 637–648.
- Fytianos, K., Siumka, A., Zachariadis, G.A., Beltsios, S., 2002. Assessment of the quality characteristics of Pinios River, Greece. *Water Air Soil Pollut.* 136 (1), 317–329.
- Gaki-Papanastassiou, K., Karymbalis, E., Maroukian, H., 2010. Recent geomorphic changes and anthropogenic activities in the deltaic plain of Pinios River in central Greece. *Bull. Geol. Soc. Greece* 43 (1), 409–417.
- Gaki-Papanastassiou, K., Cundy, A.B., Maroukian, H., 2011. Fluvial versus tectonic controls on the late Holocene geomorphic and sedimentary evolution of a small Mediterranean fan delta system. *J. Geol.* 119 (2), 221–234.
- Gámez Torrent, D., 2007. Sequence Stratigraphy as a tool for water resources management in alluvial coastal aquifers: application to the Llobregat delta (Barcelona, Spain). Universitat Politècnica de Catalunya, Doctoral Dissertation.
- Ganti, V., Chu, Z., Lamb, M.P., Nittrouer, J.A., Parker, G., 2014. Testing morphodynamic controls on the location and frequency of river avulsions on fans versus deltas: Huanghe (Yellow River), China. *Geophys. Res. Lett.* 41 (22), 7882–7890.
- Ganti, V., Chadwick, A.J., Hassenruck-Gudipati, H.J., Lamb, M.P., 2016a. Avulsion cycles and their stratigraphic signature on an experimental backwater-controlled delta. *J. Geophys. Res. Earth Surf.* 121 (9), 1651–1675.
- Ganti, V., Chadwick, A.J., Hassenruck-Gudipati, H.J., Fuller, B.M., Lamb, M.P., 2016b. Experimental river delta size set by multiple floods and backwater hydrodynamics. *Sci. Adv.* 2 (5), e1501768.
- Ghilardi, M., 2007. Dynamiques spatiales et reconstitutions paléogéographiques de la plaine de Thessalonique (Grèce) à l'Holocène récent. Doctoral dissertation. Université Paris XII Val de Marne.
- Ghilardi, M., Kunesch, S., Styllas, M., Fouache, E., 2008. Reconstruction of Mid-Holocene sedimentary environments in the central part of the Thessaloniki Plain (Greece), based on microfaunal identification, magnetic susceptibility and grain-size analyses. *Geomorphology* 97 (3–4), 617–630.
- Giosan, L., Naing, T., Min Tun, M., Clift, P.D., Filip, F., Constantinescu, S., Khonde, N., Blusztajn, J., Buylaert, J.P., Stevens, T., Thwin, S., 2018. On the Holocene evolution of the Ayeyawady megadelta. *Earth Surf. Dynam.* 6 (2), 451–466.
- Goodbred Jr., S.L., Kuehl, S.A., 2000. Enormous Ganges-Brahmaputra sediment discharge during strengthened early Holocene monsoon. *Geology* 28 (12), 1083–1086.
- Gouw, M.J., 2008. Alluvial architecture of the Holocene Rhine–Meuse delta (the Netherlands). *Sedimentology* 55 (5), 1487–1516.
- Grenfell, S.E., Ellery, W.N., Grenfell, M.C., 2009. Geomorphology and dynamics of the Mfolozi River floodplain, KwaZulu-Natal, South Africa. *Geomorphology* 107 (3–4), 226–240.
- Haghani, S., Leroy, S.A., 2020. Recent avulsion history of Sefidrud, south west of the Caspian Sea. *Quat. Int.* 540, 97–110.
- Hansford, M.R., Plink-Björklund, P., Jones, E.R., 2020. Global quantitative analyses of river discharge variability and hydrograph shape with respect to climate types. *Earth Sci. Rev.* 200, 102977.
- Hartley, A.J., Weissmann, G.S., Scuderi, L., 2017. Controls on the apex location of large deltas. *J. Geol. Soc.* 174 (1), 10–13.
- He, L., Amorosi, A., Ye, S., Xue, C., Yang, S., Laws, E.A., 2020. River avulsions and sedimentary evolution of the Luanhe fan-delta system (North China) since the late Pleistocene. *Mar. Geol.* 425, 106194.
- Heyvaert, V.M.A., Walstra, J., 2016. The role of long-term human impact on avulsion and fan development. *Earth Surf. Process. Landf.* 41 (14), 2137–2152.
- Heyvaert, V.M., Walstra, J., Verkinderen, P., Weerts, H.J., Ooghe, B., 2012. The role of human interference on the channel shifting of the Karkheh River in the Lower Khuzestan plain (Mesopotamia, SW Iran). *Quat. Int.* 251, 52–63.
- Holmes, D.A., 1968. The recent history of the Indus. *Geogr. J.* 134 (3), 367–382.
- Hoyal, D.C.J.D., Sheets, B.A., 2009. Morphodynamic evolution of experimental cohesive deltas. *J. Geophys. Res. Earth Surf.* 114, F02009.
- Hussein, M.A., 2011. Morphotectonic of Shat Al-Arab River, South of Iraq. MSc Thesis. University of Baghdad.
- Jerolmack, D.J., 2009. Conceptual framework for assessing the response of delta channel networks to Holocene sea level rise. *Quat. Sci. Rev.* 28 (17–18), 1786–1800.
- Jerolmack, D.J., Mohrig, D., 2007. Conditions for branching in depositional rivers. *Geology* 35 (5), 463–466.
- Jobe, Z.R., Howes, N.C., Straub, K.M., Cai, D., Deng, H., Laugier, F.J., Pettinga, L.A., Shumaker, L.E., 2020. Comparing aggradation, superelevation, and avulsion frequency of submarine and fluvial channels. *Front. Earth Sci.* 8, 53.
- Jones, L.S., Schumm, S.A., 1999. Causes of avulsion: an overview. In: Smith, N.D., Rogers, J. (Eds.), *Fluvial Sedimentology VI*. Wiley & Sons, pp. 169–178.
- Jones, B.G., Woodroffe, C.D., Martin, G.R., 2003. Deltas in the Gulf of Carpentaria, Australia: forms, processes, and products. In: Sidi, F.H., Nummedal, D., Imbert, P., Darman, H., Posamentier, H.W. (Eds.), *Tropical Deltas of Southeast Asia—Sedimentology, Stratigraphy, and Petroleum Geology*, 76. SEPM Special Publication, pp. 21–43.
- Kao, S.-J., Milliman, J.D., 2008. Water and sediment discharge from small mountainous rivers, Taiwan: The roles of lithology, episodic events, and human activities. *J. Geol.* 116 (5), 431–448.
- Karymbalis, E., Gaki-Papanastassiou, K., Maroukian, H., 2007. Recent geomorphic evolution of the fan delta of the Mornos river, Greece: natural processes and human impacts. *Bull. Geol. Soc. Greece* 40 (4), 1538–1551.
- Karymbalis, E., Gaki-Papanastassiou, K., Ferentinou, M., 2010. Fan deltas classification coupling morphometric analysis and artificial neural networks: The case of NW coast of Gulf of Corinth, Greece. *Hellenic J. Geosci.* 45, 133–146.
- Karymbalis, E., Gaki-Papanastassiou, K., Tsanakas, K., Ferentinou, M., 2016. Geomorphology of the Pinios River delta, Central Greece. *J. Maps* 12, 12–21.
- Karymbalis, E., Valkanou, K., Tsodoulos, I., Iliopoulos, G., Tsanakas, K., Batzakis, V., Tsironis, G., Gallousi, C., Stamoulis, K., Ioannides, K., 2018. Geomorphic Evolution of the Lilas River Fan Delta (Central Evia Island, Greece). *Geosciences* 8 (10), 361.
- Kazanci, N., Gulbazzadeh, T., 2013. Sefidrud delta and Quaternary evolution of the southern Caspian lowland, Iran. *Mar. Pet. Geol.* 44, 120–139.
- Kazanci, N., Gulbazzadeh, T., Leroy, S.A., Ileri, Ö., 2004. Sedimentary and environmental characteristics of the Gilan–Mazenderan plain, northern Iran: influence of long-and short-term Caspian water level fluctuations on geomorphology. *J. Mar. Syst.* 46 (1–4), 145–168.
- Kettner, A.J., Syvitski, J.P., 2008. HydroTrend v. 3.0: A climate-driven hydrological transport model that simulates discharge and sediment load leaving a river system. *Comput. Geosci.* 34 (10), 1170–1183.
- Kontopoulos, N., Avramidis, P., 2003. A late Holocene record of environmental changes from the Aliko lagoon, Egion, North Peloponnesus, Greece. *Quat. Int.* 111 (1), 75–90.
- Koutsios, A., Kontopoulos, N., Kalisperi, D., Soupios, P., Avramidis, P., 2010. Sedimentological and geophysical observations in the delta plain of Selinous river, ancient Helike, Northern Peloponnesus Greece. *Bull. Geol. Soc. Greece* 43 (2), 654–662.
- Kravtsova, V.I., Mikhailov, V.N., Kidyayeva, V.M., 2009. Hydrological regime, morphological features and natural territorial complexes of the Irrawaddy River Delta (Myanmar). *Water Res.* 36 (3), 243–260.
- Lamb, M.P., Nittrouer, J.A., Mohrig, D., Shaw, J., 2012. Backwater and river plume controls on scour upstream of river mouths: implications for fluvio-deltaic morphodynamics. *J. Geophys. Res. Earth Surf.* 117, F01002.
- Lambeck, K., Rouby, H., Purcell, A., Sun, Y., Sambridge, M., 2014. Sea level and global ice volumes from the Last Glacial Maximum to the Holocene. *Proc. Natl. Acad. Sci.* 111 (43), 15296–15303.
- Lane, T.L., Nanson, R.A., Vakarelov, B.K., Ainsworth, R.B., Dashtgard, S.E., 2017. Evolution and architectural styles of a forced-regressive Holocene delta and megafan, Mitchell River, Gulf of Carpentaria, Australia. In: Hampson, G.J., Reynolds, A.D., Kostic, B., Wells, M.R. (Eds.), *Sedimentology of Paralic Reservoirs: Recent Advances*, 444. Geological Society, London, Special Publications, pp. 305–334.
- Mackey, S.D., Bridge, J.S., 1995. Three-dimensional model of alluvial stratigraphy; theory and applications. *J. Sediment. Res.* 65 (1b), 7–31.
- Maejima, W., Mahalik, N.K., 2002. Control of prevalent wind on the development of distributary channel systems of Mahanadi delta, India. *J. Sedimentol. Soc. Japan* 55, 1–8.
- Mahalik, N.K., Das, C., Maejima, W., 1996. Geomorphology and evolution of the Mahanadi Delta, India. *J. Geosci. Osaka City Univ.* 39, 111–122.
- Maroukian, H., Karymbalis, E., 2004. Geomorphic evolution of the fan delta of the Evinos river in western Greece and human impacts in the last 150 years. *Z. Geomorphol.* 201–217.
- Martin, L., Suguio, K., Flexor, J.M., 1993. As flutuações de nível do mar durante o quaternário superior e a evolução geológica de “deltas” brasileiros. *Boletim IG-USP, Publicação Especial* 15, 1–186.
- Mateo, Z.R.P., Siringan, F.P., 2007. Tectonic control of high-frequency Holocene delta switching and fluvial migration in Lingayen Gulf bayhead, northwestern Philippines. *J. Coast. Res.* 23 (1), 182–194.
- Mathers, S., Zalasiewicz, J., 1999. Holocene sedimentary architecture of the Red River delta, Vietnam. *J. Coast. Res.* 314–325.
- McCarthy, T.S., Ellery, W.N., Stanistreet, I.G., 1992. Avulsion mechanisms on the Okavango fan, Botswana: the control of a fluvial system by vegetation. *Sedimentology* 39 (5), 779–795.
- McGowen, J.H., Proctor, C.V., Brown Jr., L.F., Evans, T.J., Fisher, W.L., Groat, C.G., 1976. Environmental geologic atlas of the Texas coastal zone—Port Lavaca area: The University of Texas at Austin. Bureau Econ. Geol. 107.
- Meybeck, M., Laroche, L., Dürr, H.H., Syvitski, J.P.M., 2003. Global variability of daily total suspended solids and their fluxes in rivers. *Glob. Planet. Chang.* 39 (1–2), 65–93.
- Mikhailov, V.N., Kravtsova, V.I., Magritskii, D.V., 2004. Specific features of development of the modern Sulak River Delta. *Water Res.* 31 (2), 117–132.
- Mikhailov, V.N., Magritskiy, D.V., Kravtsova, V.I., Mikhailova, M.V., Isupova, M.V., 2012. The response of river mouths to large-scale variations in sea level and river runoff: Case study of rivers flowing into the Caspian Sea. *Water Res.* 39 (1), 11–43.
- Milliman, J.D., Farnsworth, K.L., 2011. *River Discharge to the Coastal Ocean: A Global Synthesis*. Cambridge University Press.
- Moodie, A.J., Nittrouer, J.A., Ma, H., Carlson, B.N., Chadwick, A.J., Lamb, M.P., Parker, G., 2019. Modeling deltaic lobe-building cycles and channel avulsions for the Yellow River delta, China. *J. Geophys. Res. Earth Surf.* 124 (11), 2438–2462.
- Moran, K.E., Nittrouer, J.A., Perillo, M.M., Lorenzo-Trueba, J., Anderson, J.B., 2017. Morphodynamic modeling of fluvial channel fill and avulsion time scales during

- early Holocene transgression, as substantiated by the incised valley stratigraphy of the Trinity River, Texas. *J. Geophys. Res. Earth Surf.* 122, 215–234.
- Mörner, N.-A., 2013. Sea level changes past records and future expectations. *Energy & Environ.* 24 (3–4), 509–536.
- Morozova, G.S., Smith, N.D., 1999. Holocene Avulsion History of the Lower Saskatchewan Fluvial System, Cumberland Marshes, Saskatchewan–Manitoba, Canada. In: Smith, N.D., Rogers, J. (Eds.), *Fluvial Sedimentology*, VI. Wiley & Sons, pp. 231–249.
- Morozova, G.S., Smith, N.D., 2000. Holocene avulsion styles and sedimentation patterns of the Saskatchewan River, Cumberland Marshes, Canada. *Sediment. Geol.* 130 (1–2), 81–105.
- Mulrennan, M.E., Woodroffe, C.D., 1998. Holocene development of the lower Mary River plains, Northern Territory, Australia. *The Holocene* 8 (5), 565–579.
- Muñoz-Salinas, E., Castillo, M., Sanderson, D., Kinnaird, T., 2017. Geochronology and landscape evolution of the strand-plain of the Usumacinta and Grijalva rivers, southern Mexico. *J. S. Am. Earth Sci.* 79, 394–400.
- Muto, T., Steel, R.J., 1992. Retreat of the front in a prograding delta. *Geology* 20 (11), 967–970.
- Nageswara Rao, K., Saito, Y., Nagakumar, K.C.V., Demudu, G., Rajawat, A.S., Kubo, S., Li, Z., 2015. Palaeogeography and evolution of the Godavari delta, east coast of India during the Holocene: an example of wave-dominated and fan-delta settings. *Palaeogeogr. Palaeoclimatol. Palaeoecol.* 440, 213–233.
- Nageswara Rao, K., Saito, Y., Kumar, K.C.V.N., Kubo, S., Pandey, S., Li, Z., Demudu, G., Rajawat, A.S., 2020. Holocene evolution and Anthropocene destruction of the Krishna Delta on the east coast of India: delta lobe shifts, human impacts, and sea-level history. *Mar. Geol.* 427, 106229.
- Nanson, G.C., Price, D.M., Short, S.A., Young, R.W., Jones, B.G., 1991. Comparative uranium-thorium and thermoluminescence dating of weathered Quaternary alluvium in the tropics of northern Australia. *Quat. Res.* 35 (3–Part1), 347–366.
- Nienhuis, J.H., Ashton, A.D., Edmonds, D.A., Houtink, A.J.F., Kettner, A.J., Rowland, J.C., Törnqvist, T.E., 2020. Global-scale human impact on delta morphology has led to net land area gain. *Nature* 577, 514–518.
- Nijhuis, A.G., 2013. Fluvio-deltaic response to relative sea-level fall: A case study of the Goose River delta, Labrador, Canada. MSc Thesis, Boston College.
- Nijhuis, A.G., Edmonds, D.A., Caldwell, R.L., Cederberg, J.A., Slingerland, R.L., Best, J.L., Parsons, D.R., Robinson, R.A.J., 2015. Fluvio-deltaic avulsions during relative sea-level fall. *Geology* 43 (8), 719–722.
- Nooren, K., 2017. Holocene evolution of the Tabasco delta–Mexico: impact of climate, volcanism and humans. In: *Utrecht Studies in Earth Sciences*, 144. Utrecht University.
- Nooren, K., Hoek, W.Z., Winkels, T., Huizinga, A., Van der Plicht, H., Van Dam, R.L., Van Heteren, S., Van Bergen, M.J., Prins, M.A., Reimann, T., Wallinga, J., Cohen, K.M., Minderhoud, P., Middelkoop, H., 2017. The Usumacinta–Grijalva beach-ridge plain in southern Mexico: a high-resolution archive of river discharge and precipitation. *Earth Surf. Dynam.* 5 (3), 529–556.
- Oldfield, F., Dearing, J.A., 2003. The role of human activities in past environmental change. In: Alverson, K.D., Bradley, R.S., Pedersen, T.F. (Eds.), *Paleoclimate, Global Change and the Future*. Springer, Berlin, Heidelberg, pp. 143–162.
- Paola, C., 2000. Quantitative models of sedimentary basin filling. *Sedimentology* 47 (s1), 121–178.
- Parcharidis, I., Kourkoulis, P., Karymbalis, E., Fomelis, M., Karathanassi, V., 2013. Time series synthetic aperture radar interferometry for ground deformation monitoring over a small scale tectonically active deltaic environment (Mornos, Central Greece). *J. Coast. Res.* 29 (2), 325–338.
- Pelletier, J.D., Turcotte, D.L., 1997. Synthetic stratigraphy with a stochastic diffusion model of fluvial sedimentation. *J. Sediment. Res.* 67 (6), 1060–1067.
- Pennington, B.T., Sturt, F., Wilson, P., Rowland, J., Brown, A.G., 2017. The fluvial evolution of the Holocene Nile Delta. *Quat. Sci. Rev.* 170, 212–231.
- Phillips, J.D., 2012. Log-jams and avulsions in the San Antonio River delta, Texas. *Earth Surf. Process. Landf.* 37 (9), 936–950.
- Piper, D.J.W., Panagos, A.G., 1981. Growth patterns of the Acheloos and Evinos deltas, western Greece. *Sediment. Geol.* 28 (2), 111–132.
- Potemkina, T.G., 2011. Sediment runoff formation trends of major tributaries of Lake Baikal in the 20th century and at the beginning of the 21<sup>st</sup> century. *Russ. Meteorol. Hydrol.* 36 (12), 819–825.
- Poulos, S.E., Chronis, G., 1997. The importance of the river systems in the evolution of the Greek coastline. *Bull. l'Institut Océanogr. (Monaco)* 18, 75–96.
- Powell, E.J., Kim, W., Muto, T., 2012. Varying discharge controls on timescales of autogenic storage and release processes in fluvio-deltaic environments: Tank experiments. *J. Geophys. Res. Earth Surf.* 117, F02011.
- Provansal, M., Pichard, G., Anthony, E.J., 2015. Geomorphic changes in the Rhône delta during the LIA: input from the analysis of ancient maps. In: Maanan, M., Robin, M. (Eds.), *Sediment Fluxes in Coastal Areas*. Springer, Dordrecht, pp. 47–72.
- Pueppke, S.G., Nurtazin, S.T., Graham, N.A., Qi, J., 2018. Central Asia's Ili River ecosystem as a wicked problem: unraveling complex interrelationships at the interface of water, energy, and food. *Water* 10 (5), 541.
- Quigley, M., Duffy, B., 2020. Effects of earthquakes on flood hazards: a case study from Christchurch, New Zealand. *Geosciences* 10 (3), 114.
- Ramasamy, S.M., Bakliwal, P.C., Verma, R.P., 1991. Remote sensing and river migration in Western India. *Int. J. Remote Sens.* 12 (12), 2597–2609.
- Ramasamy, S.M., Saravanan, J., Yadava, M.G., Ramesh, R., 2006. Radiocarbon dating of some palaeochannels in Tamil Nadu and their significance. *Curr. Sci.* 91 (12), 1609–1613.
- Ratliff, K.M., Hutton, E.H., Murray, A.B., 2018. Exploring wave and sea-level rise effects on delta morphodynamics with a coupled river-ocean model. *J. Geophys. Res. Earth Surf.* 123 (11), 2887–2900.
- Ratliff, K.M., Hutton, E.W., Murray, A.B., 2021. Modeling long-term delta dynamics reveals persistent geometric river avulsion locations. *Earth Planet. Sci. Lett.* 559, 116786.
- Reitz, M.D., Jerolmack, D.J., 2012. Experimental alluvial fan evolution: channel dynamics, slope controls, and shoreline growth. *J. Geophys. Res. Earth Surf.* 117, F02021.
- Reitz, M.D., Jerolmack, D.J., Swenson, J.B., 2010. Flooding and flow path selection on alluvial fans and deltas. *Geophys. Res. Lett.* 37 (6), L06401.
- Reitz, M.D., Pickering, J.L., Goodbred, S.L., Paola, C., Steckler, M.S., Seeber, L., Akhter, S.H., 2015. Effects of tectonic deformation and sea level on river path selection: theory and application to the Ganges-Brahmaputra-Meghna River Delta. *J. Geophys. Res. Earth Surf.* 120 (4), 671–689.
- Resmi, M.R., Achyuthan, H., Jaiswal, M.K., 2017. Middle to late Holocene paleochannels and migration of the Palar River, Tamil Nadu: implications of neotectonic activity. *Quat. Int.* 443, 211–222.
- Restrepo, J.D., Cantera, J.R., 2013. Discharge diversion in the Patia River delta, the Colombian Pacific: geomorphic and ecological consequences for mangrove ecosystems. *J. S. Am. Earth Sci.* 46, 183–198.
- Rey, T., Lefevre, D., Vella, C., 2009. Deltaic plain development and environmental changes in the Petite Camargue, Rhone Delta, France, in the past 2000 years. *Quat. Res.* 71 (3), 284–294.
- Rivera, P.C., 1997. Hydrodynamics, Sediment Transport and Light Extinction off Cape Bolinao, Philippines. Wageningen Agricultural University, Doctoral Dissertation.
- Roberts, H.H., 1997. Dynamic changes of the Holocene Mississippi River delta plain: the delta cycle. *J. Coast. Res.* 13 (3), 605–627.
- Rossetti, D.F., Polizel, S.P., Cohen, M.C.L., Pessenda, L.C.R., 2015. Late Pleistocene–Holocene evolution of the Doce River delta, southeastern Brazil: implications for the understanding of wave-influenced deltas. *Mar. Geol.* 367, 171–190.
- Rossi, V.M., Kim, W., Leva López, J., Edmonds, D., Geleynse, N., Olariu, C., Steel, R.J., Hiatt, M., Passalacqua, P., 2016. Impact of tidal currents on delta-channel deepening, stratigraphic architecture, and sediment bypass beyond the shoreline. *Geology* 44 (11), 927–930.
- Ruiz-Pérez, J.M., Carmona, P., 2019. Turia river delta and coastal barrier-lagoon of Valencia (Mediterranean coast of Spain): geomorphological processes and global climate fluctuations since Iberian-Roman times. *Quat. Sci. Rev.* 219, 84–101.
- Rustomji, P., 2010. A statistical analysis of flood hydrology and bankfull discharge for the Mitchell River catchment, Queensland, Australia. Water for a Healthy Country National Research Flagship (01/2010). CSIRO, Canberra.
- Rutishauser, S., Erasmí, S., Rosenbauer, R., Buchbach, R., 2017. SAR archaeology—Detecting palaeochannels based on high resolution radar data and their impact of changes in the settlement pattern in Cilicia (Turkey). *Geosciences* 7 (4), 109.
- Sadler, P.M., 1981. Sediment accumulation rates and the completeness of stratigraphic sections. *J. Geol.* 89 (5), 569–584.
- Sadler, P.M., Jerolmack, D.J., 2015. Scaling laws for aggradation, denudation and progradation rates: the case for time-scale invariance at sediment sources and sinks. In: Smith, D.G., Bailey, R.J., Burgess, P.M., Fraser, A.J. (Eds.), *Strata and Time: Probing the Gaps in our Understanding*, 404. Geological Society, London, Special Publications, pp. 69–88.
- Sarker, M.H., Akter, J., Rahman, M.M., 2013. Century-scale dynamics of the Bengal Delta and future development. In: *Proceedings of the 4<sup>th</sup> International Conference on Water and Flood Management*, pp. 91–104.
- Serrano Suarez, B.E., 2004. The Sinú river delta on the northwestern Caribbean coast of Colombia: Bay infilling associated with delta development. *J. S. Am. Earth Sci.* 16 (7), 623–631.
- Shi, C., Dian, Z., You, L., 2002. Changes in sediment yield of the Yellow River basin of China during the Holocene. *Geomorphology* 46 (3–4), 267–283.
- Singh, P., Yadava, M.G., Ahmad, M.Z., Mohapatra, P.P., Laskar, A.H., Doradla, S., Saravanan, J., Kumanan, C.J., 2015. Fertile farmlands in Cauvery delta: evolution through LGM. *Curr. Sci.* 218–225.
- Skoulikidis, N., Dimitriou, E., Karaouzas, I., 2018. The Rivers of Greece. Springer, Berlin/Heidelberg, Germany.
- Slingerland, R., Smith, N.D., 2004. River avulsions and their deposits. *Annu. Rev. Earth Planet. Sci.* 32, 257–285.
- Smith, D.E., Harrison, S., Firth, C.R., Jordan, J.T., 2011. The early Holocene sea level rise. *Quat. Sci. Rev.* 30 (15–16), 1846–1860.
- Somoza, L., Rodríguez-Santalla, I., 2014. Geology and geomorphological evolution of the Ebro River Delta. In: Gutiérrez, F., Gutiérrez, M. (Eds.), *Landscapes and Landforms of Spain*. Springer, Dordrecht, pp. 213–227.
- Somoza, L., Barnolas, A., Arasa, A., Maestro, A., Rees, J.G., Hernández-Molina, F.J., 1998. Architectural stacking patterns of the Ebro delta controlled by Holocene high-frequency eustatic fluctuations, delta-lobe switching and subsidence processes. *Sediment. Geol.* 117 (1–2), 11–32.
- Stanley, D.J., Warne, A.G., 1993. Nile Delta: recent geological evolution and human impact. *Science* 260, 628–634.
- Stanley, J.D., Warne, A.G., Schnepf, G., 2004. Geoarchaeological interpretation of the Canopic, largest of the relict Nile Delta distributaries, Egypt. *J. Coast. Res.* 20 (3), 920–930.
- Stouthamer, E., Berendsen, H.J., 2000. Factors controlling the Holocene avulsion history of the Rhine-Meuse delta (The Netherlands). *J. Sediment. Res.* 70 (5), 1051–1064.
- Stouthamer, E., Berendsen, H.J., 2001. Avulsion frequency, avulsion duration, and interavulsion period of Holocene channel belts in the Rhine-Meuse delta, the Netherlands. *J. Sediment. Res.* 71 (4), 589–598.
- Stouthamer, E., Berendsen, H.J., 2007. Avulsion: the relative roles of autogenic and allogenic processes. *Sediment. Geol.* 198 (3–4), 309–325.

- Stouthamer, E., Cohen, K.M., Gouw, M.J.P., 2011. Avulsion and its implications for fluvial-deltaic architecture: insights from the Holocene Rhine-Meuse delta. In: Davidson, S.K., Leleu, S., North, C.P. (Eds.), *From River To Rock Record: The Preservation Of Fluvial Sediments And Their Subsequent Interpretation*, 97. SEPM Special Publication, pp. 215–231.
- Styllas, M., 2018. Natural processes versus human impacts during the last century: A case study of the Aliakmon River Delta. In: Skoulikidis, N., Dimitriou, E., Karaouzas, I. (Eds.), *The Rivers of Greece*. Springer, Berlin, Heidelberg, pp. 31–49.
- Swenson, J.B., 2005. Relative importance of fluvial input and wave energy in controlling the timescale for distributary-channel avulsion. *Geophys. Res. Lett.* 32, L23404.
- Syvitski, J.P., Kettner, A., 2011. Sediment flux and the anthropocene. *Philos. Trans. R. Soc. A Math. Phys. Eng. Sci.* 369, 957–975.
- Syvitski, J.P., Saito, Y., 2007. Morphodynamics of deltas under the influence of humans. *Glob. Planet. Chang.* 57 (3–4), 261–282.
- Syvitski, J.P., Kettner, A.J., Overeem, I., Giosan, L., Brakenridge, G.R., Hannon, M., Bilham, R., 2013. Anthropocene metamorphosis of the Indus Delta and lower floodplain. *Anthropocene* 3, 24–35.
- Tamura, T., Saito, Y., Nguyen, V.L., Ta, T.O., Bateman, M.D., Matsumoto, D., Yamashita, S., 2012. Origin and evolution of interdistributary delta plains; insights from Mekong River delta. *Geology* 40, 303–306.
- Tanabe, S., Saito, Y., Vu, Q.L., Hanebuth, T.J., Ngo, Q.L., Kitamura, A., 2006. Holocene evolution of the Song Hong (Red River) delta system, northern Vietnam. *Sediment. Geol.* 187 (1–2), 29–61.
- Törnqvist, T.E., 1994. Middle and late Holocene avulsion history of the River Rhine (Rhine-Meuse delta, Netherlands). *Geology* 22 (8), 711–714.
- Törnqvist, T.E., Bridge, J.S., 2002. Spatial variation of overbank aggradation rate and its influence on avulsion frequency. *Sedimentology* 49 (5), 891–905.
- Törnqvist, T.E., Kidder, T.R., Autin, W.J., van der Borg, K., de Jong, A.F., Klerks, C.J., Snijders, E.M.A., Storms, J.E.A., van Dam, R.L., Wiemann, M.C., 1996. A revised chronology for Mississippi River subdeltas. *Science* 273 (5282), 1693–1696.
- Van Andel, T.H., 1967. The Orinoco delta. *J. Sediment. Res.* 37 (2), 297–310.
- van Asselen, S., Stouthamer, E., Van Asch, T.W., 2009. Effects of peat compaction on delta evolution: a review on processes, responses, measuring and modeling. *Earth Sci. Rev.* 92, 35–51.
- van Gelder, A., van den Berg, J.H., Cheng, G., Xue, C., 1994. Overbank and channelfill deposits of the modern Yellow River delta. *Sediment. Geol.* 90 (3–4), 293–305.
- Vespremeanu-Stroe, A., Preoteasa, L., Zăinescu, F., Tătui, F., 2017a. The evolution of Danube delta after Black Sea reconnection to World Ocean. In: Radoane, M., Vespremeanu-Stroe, A. (Eds.), *Landform Dynamics and Evolution in Romania*. Springer, Cham, pp. 521–549.
- Vespremeanu-Stroe, A., Zăinescu, F., Preoteasa, L., Tătui, F., Rotaru, S., Morhange, C., Stoica, M., Hanganu, J., Timar-Gabor, A., Cărdan, I., Piotrowska, N., 2017b. Holocene evolution of the Danube delta: An integral reconstruction and a revised chronology. *Mar. Geol.* 388, 38–61.
- von Nagy, C., 2011. Coastal deltaic dynamics, human settlement, and ancient Olmec polities in Tabasco, Mexico. In: 76<sup>th</sup> Annual Meeting of the Society For American Archaeology, Sacramento, California, April 1, 2011.
- Vött, A., Schriever, A., Handl, M., Brückner, H., 2007a. Holocene palaeogeographies of the central Acheloos River delta (NW Greece) in the vicinity of the ancient seaport Oiniadai. *Geodin. Acta* 20 (4), 241–256.
- Vött, A., Schriever, A., Handl, M., Brückner, H., 2007b. Holocene palaeogeographies of the eastern Acheloos River delta and the Lagoon of Etoliko (NW Greece). *J. Coast. Res.* 23 (4), 1042–1066.
- Walling, D.E., 1983. The sediment delivery problem. In: Rodríguez-Iturbe, I., & Gupta, V. K. (Eds.), *scale problems in hydrology*. *J. Hydrol.* 65 (1–3), 209–237.
- Walling, D.E., 2011. Human impact on the sediment loads of Asian rivers. In: *Sediment Problems and Sediment Management in Asian River Basins*, IAHS Publication, 349. IAHS Press, Wallingford, pp. 37–51.
- Wang, Y., Ren, M.E., Zhu, D., 1986. Sediment supply to the continental shelf by the major rivers of China. *J. Geol. Soc.* 143 (6), 935–944.
- Wang, Y., Liu, X., Li, G., Zhang, W., 2016. Stratigraphic variations in the Diaokou lobe area of the Yellow River delta, China: implications for an evolutionary model of a delta lobe. In: Clift, P.D., Harff, J., Wu, J., Qui, Y. (Eds.), *River-Dominated Shelf Sediments of East Asian Seas*, 429. Geological Society, London, Special Publications, pp. 185–195.
- Weinstein, R.A., Junkin, G.M., 1992. Natural setting. In: Weinstein, R.A. (Ed.), *Archaeology and Paleogeography of the Lower Guadalupe River/San Antonio Bay Region: Cultural Resources Investigations Along the Channel to Victoria, Calhoun and Victoria Counties, Texas*. Coastal Environments, Inc, Baton Rouge, pp. 7–22.
- Welder, F.A., 1955. Deltaic processes in Cubits Gap area, Plaquemines Parish, Louisiana. Doctoral Dissertation. Louisiana State University and Agricultural & Mechanical College.
- Woodroffe, C.D., Chappell, J., 1993. Holocene emergence and evolution of the McArthur River Delta, southwestern Gulf of Carpentaria, Australia. *Sediment. Geol.* 83 (3–4), 303–317.
- Zheng, S., Wu, B., Wang, K., Tan, G., Han, S., Thorne, C.R., 2017. Evolution of the Yellow River delta, China: Impacts of channel avulsion and progradation. *Int. J. Sediment Res.* 32 (1), 34–44.